

1 **Sea ice and pollution-modulated changes in Greenland ice core**
2 **methanesulfonate and bromine**

3 **O.J. Maselli^{1*}, N.J. Chellman¹, M. Grieman², L. Layman¹, J. R. McConnell¹, D. Pasteris¹,**
4 **R.H. Rhodes³, E. Saltzman², M. Sigl¹**

5 [1] {Desert Research Institute, Department of Hydrologic Sciences, Reno, NV, USA}

6 [2] {University of California Irvine, Department of Earth System Science, Irvine, CA, USA}

7 [3] {University of Cambridge, Department of Earth Sciences, Cambridge, UK}

8 [*] {now at: The University of Adelaide, Australia, 5000}

9 *Correspondence to:* Olivia Maselli (olivia.maselli@adelaide.edu.au)

10

11 **Keywords:** bromine, MSA, nitrate, sea ice, pollution, acidification, Arctic, Greenland, cryosphere

12

13 **Abstract**

14 Reconstruction of past changes in Arctic sea ice extent may be critical for understanding its future
15 evolution. Methanesulphonate (MSA) and bromine concentrations preserved in ice cores have both
16 been proposed as indicators of past sea ice conditions. In this study, two ice cores from central and NE
17 Greenland were analysed at sub-annual resolution for MSA (CH_3SO_3H) and bromine, covering the time
18 period 1750-2010. We examine correlations between ice core MSA and the HadISST1 ICE sea ice
19 dataset and consult back-trajectories to infer the likely source regions. A strong correlation between the
20 low frequency MSA and bromine records during preindustrial times indicates that both chemical species
21 are likely linked to processes occurring on or near sea ice in the same source regions. The positive
22 correlation between ice core MSA and bromine persists until the mid-20th century, when the acidity of
23 Greenland ice begins to increase markedly due to increased fossil fuel emissions. After that time, MSA
24 levels decrease as a result of declining sea ice extent but bromine levels increase. We consider several
25 possible explanations and ultimately suggest that increased acidity, specifically nitric acid, of snow on
26 sea ice stimulates the release of reactive Br from sea ice, resulting in increased transport and deposition
27 on the Greenland ice sheet.

29 1 Introduction

30 Atmospheric chemistry in the polar regions is strongly modulated by physical, chemical, and biological
31 processes occurring in and around sea ice. These include sea salt aerosol generation, biogenic emissions
32 of sulfur-containing gases and halogenated organics, and the photochemical/heterogeneous reactions
33 leading to release of volatile, reactive bromine species. The resulting chemical signals influence the
34 chemistry of the aerosol deposited on polar ice sheets. For this reason ice core measurements of sea salt
35 ions, methanesulphonate (MSA), and bromine have been examined as potential tracers for sea ice extent
36 (Abram et al., 2013; Spolaor et al., 2013b, 2016; Wolff et al., 2003). The interpretation of such tracers
37 is complicated by the fact that their source functions reflect changes in highly complex systems, and
38 signals are further modified by patterns of atmospheric transport and deposition.

39 MSA is produced by the atmospheric oxidation of DMS ($(CH_3)_2S$). DMS is produced throughout the
40 world's oceans as a breakdown product of the algal metabolite DMSP, ($(CH_3)_2S^+CH_2CH_2COO^-$).
41 DMS emissions are particularly strong in marginal sea ice zones (Sharma et al., 2012), and this source
42 is believed to be a dominant contributor to the MSA signal in polar ice (Curran and Jones, 2000). Ice
43 core MSA records have been used extensively in Antarctica as a proxy for local sea ice dynamics.
44 Although the specifics of the relationship are highly site-dependent (Abram et al., 2013; Curran et al.,
45 2003) MSA has been proven to be a reasonably good proxy for sea ice conditions (e.g., (Curran and
46 Jones, 2000)). In the Arctic, the relationship between MSA and sea ice conditions is less straightforward
47 due to the likelihood of multiple source regions with different sea ice conditions contributing to the ice
48 core archived MSA (Abram et al., 2013). Until now, a significant, ($r = -0.66$) relationship between ice
49 core MSA and Arctic sea ice extent (specifically August in the Barents sea) has only been established
50 for a short record from a Svalbard ice core (O'Dwyer et al., 2000). In this study we analyse the direct
51 correlations between the MSA records from two Greenland ice core sites and the surrounding sea ice
52 conditions in order to demonstrate the utility of MSA as a local sea ice proxy.

53 In this study, all dissolved or suspended bromine species are measured (including organic bromine) and
54 shall be referred to as "bromine". The primary source of total inorganic bromine (e.g. Br_2 , Br^- , HBr)
55 in the marine boundary layer (MBL) is the ocean (Parrella et al., 2012; Sander et al., 2003). At
56 concentrations of less than 0.2% that of sodium (Na), bromide (Br^-) makes a small contribution to
57 ocean salinity. Br^- can be concentrated in the high latitude oceans when the sea water is frozen, since
58 the formation of the ice matrix exudes the sea-salts in the form of brine (Abbatt et al., 2012). Small, sea-
59 salt aerosol particles blown from the surface of sea ice are typically enriched with bromine (Sander et

60 al., 2003) and satellite imagery has revealed that plumes of bromine (as BrO) are photo-chemically
61 released from sea-ice zones in spring (Nghiem et al., 2012; Schönhardt et al., 2012; Wagner et al., 2001).
62 Recently, studies have begun to link ice core records of bromide enrichment (relative to sea water *Na*
63 concentrations) preserved in polar ice sheets to that of local sea ice conditions (Spolaor et al., 2013a,
64 2013b, 2014). Spolaor and co-workers demonstrated the spring-time Br^-/Na that is preserved in the
65 ice core is a record of bromine explosion events over adjacent seasonal sea ice. A Br^-/Na enrichment
66 would therefore indicate a larger seasonal sea ice extent or conversely a shorter distance between the
67 ice edge and the ice core site due to decreased multi-year sea ice (Spolaor et al., 2013a). However, like
68 MSA, it is likely that the bromine – sea-ice relationship in the Arctic is complicated by the myriad of
69 bromine source regions which influence an ice core record in addition to factors which influence the
70 degree of enrichment of the aerosol as it travels to the ice core site. In this study we compare ice core
71 records of bromine to those of MSA and other common MBL species in order to determine the influence
72 of sea ice conditions and other factors on bromine concentrations.

73 Here we present measurements of MSA, bromine, and elemental tracers of sea salt and crustal input in
74 two Greenland ice cores covering the time period 1750-2010 C.E.. These ice core records represent the
75 first continuous, sub-annual resolution records of bromine in polar ice to extend beyond the satellite era.
76 We examine the relationship between these two sea ice-modulated tracers, their relationship to
77 independent historical estimates of sea ice distribution, and the influence of industrialization on
78 atmospheric and ice core chemistry.

79 **2 Methods**

80 **2.1 Ice cores**

81 The 87 m ‘Summit-2010’ ice core was collected in 2010 close to Summit Station, Greenland (72°20'N
82 38°17'24"W, Fig. 1). The average snow accumulation at Summit, as determined from the ice core
83 record, is $\sim 0.22 \text{ m yr}^{-1}$ water equivalent, with few instances of melt. Due to the relatively high snow
84 accumulation rate, seasonal analysis of the sea salt species concentrations was feasible. The 213 m Tunu
85 core was collected in 2013 (78° 2' 5.5"N, 33° 52' 48"W, Fig. 1), approximately 3 km east of the Tunu-
86 N automatic weather station, part of the Greenland Climate Network. The average snow accumulation
87 at Tunu, as determined from the ice core record, is $\sim 0.11 \text{ m yr}^{-1}$ water equivalent.

88 The Summit-2010 and Tunu cores were dated using volcanic horizons in sulfur (S) from well dated
89 historic eruptions (e.g., 1815, 1835, 1846, 1854, 1873, 1883, 1912). The dating of both cores was refined
90 by annual layer counting using seasonal cycles in Na, Ca, and the ratio of non-sea salt S/Na as described

91 in more detail for another Greenland ice core (NEEM-2011-S1) by Sigl et al., (2013, 2015). Annual-
92 layer boundaries (nominal January) were defined as the minimum value in the ratio of non-sea salt S/Na
93 following Sigl et al. (2013). The seasonal cycles in Na and Ca (from sea-salt and mineral dust emissions
94 peaking in winter months) remain largely unaffected by rising anthropogenic emissions during the
95 industrial period and thus can be used for annual layer counting for the entire record. The minimum in
96 hydrogen peroxide was also used as a winter marker in the upper section of the Summit-2010 core.
97 Timing was evaluated for consistency against other parameters including insoluble particle counts and
98 black carbon. Monthly values were calculated assuming a constant distribution of snowfall within each
99 year. Because of the lower accumulation rate and strong katabatic winds at the Tunu site, constraints
100 from volcanic synchronization played a more important role in the developing the depth-age scale for
101 the Tunu core compared with Summit-2010. First the Tunu non-sea salt S record was synchronized to
102 the NEEM-2011-S1 volcanic record (Sigl et al., 2015) and then the required number of annual layers
103 between volcanic horizons picked from the high-resolution chemistry.
104 The annual-layer dating for these ice cores resulted in a plutonium record that is consistent with other
105 ice cores from Greenland between 1950 and 1970 and with the emission histories from nuclear weapon
106 testing in the Northern Hemisphere (Arienzo et al., 2016). The error in the dating of the ice core records
107 was estimated as ± 0.33 years for the Summit-2010 record and ± 1 years for the Tunu record.

108 **2.2 Sampling and analysis**

109 The ice cores were sampled from 33x33 mm cross-section sticks using a continuous melter system
110 (McConnell et al., 2002). The silicon carbide melter plate provides three streams from concentric square
111 regions of the ice core sample: an innermost stream (with a cross sectional area of 144 mm²), an
112 intermediate stream (340 mm²) and an outer stream that was discarded along with any contaminants
113 obtained from handling of the ice core. The innermost melt stream was directed to two inductively
114 coupled plasma-mass spectrometers (ICP-MS, Thermo Element II high resolution with PFA-ST
115 concentric Teflon nebulizer (ESI)) run in parallel. All calibrations and runtime standards were run on
116 both instruments and several elements were also measured in duplicate (Na, Ce, Pb) to ensure tracking
117 between both ICP-MS. In addition, an internal standard of yttrium flowed through the entire analytical
118 system and was used to observe any change in system sensitivity. The instrument measuring bromine
119 was run at medium resolution and there were no mass interferences observed at the bromine isotope
120 mass monitored (79 amu). The sample stream was acidified to 1% *HNO*₃ to prevent loss of less soluble
121 species, degassed just prior to analysis to minimize mixing in the sample line and sampled at a rate of
122 0.45ml min⁻¹ (McConnell et al., 2002; Sigl et al., 2013). The following elements were measured by

123 ICP-MS: Br, Cl, Na, Ca, S, Ce, and Pb. Calibration of the ICP-MS was based on a series of 7 mixed
124 standards measured at the start and end of each day for all elements except for the halides. Due to the
125 high volatility of acid halides, a set of 4 bromine and chlorine standards were made individually in a
126 1% UHP HNO_3 matrix from fresh, non-acidified intermediate stock solution (Inorganic Ventures) every
127 day. The intermediate melt stream was directed to a continuous flow analysis (CFA) system on which
128 nitrate ion (NO_3^-) and snow acidity (sum of soluble acidic species) were measured using the technique
129 described by Pasteris (2012) in addition to other atmospheric species of interest (Röthlisberger et al.,
130 2000). Stable water isotopes records were also collected using the CFA system according to the method
131 described by Maselli et al. (2013)

132 The analysis of MSA by batch analysis using ESI/MS/MS has been reported previously (Saltzman et
133 al., 2006). A portion of the debubbled CFA melt stream ($150 \mu l \text{ min}^{-1}$) was subsampled for continuous
134 on-line analysis of methanesulfonate by electrospray triple-quad mass spectrometer (ESI/MS/MS;
135 Thermo-Finnigan Quantum). This subsample was mixed with pure methanol ($50 \mu l \text{ min}^{-1}$) delivered
136 using an M6 pump (syringe-free liquid handling pump, VICI). The methanol was spiked with an
137 internal standard of deuterated MSA ($CD_3SO_3^-$; Cambridge Isotopes) at a concentration of 52 nM. The
138 internal isotope standard was used to correct for any changes in instrument response due to variations
139 in water chemistry (such as acidity). The isotope standard was calibrated against non-deuterated MSA
140 standards prepared in water from non-deuterated MSA ($CH_3SO_3^-$; Sigma Aldrich). MSA was detected
141 in negative ion mode using the $CH_3SO_3^-/SO_3^-$ transition (m/z 95/80) and $CD_3SO_3^-/SO_3^-$ (m/z 98/80). The
142 concentration of MSA in the sample flow was determined from the ratio of the non-deuterated and
143 deuterated signals after minor blank corrections. This study is the first use of the technique for ice core
144 MSA analysis in a continuous, online mode. The uncertainty in the MSA intensity as calculated from
145 the standard calibrations is 1%.

146 A second portion of the debubbled CFA melt stream was directed to an autosampler collection system
147 to collect a discretely sampled archive of the melted ice cores. The collected samples were frozen at the
148 end of each day and later analysed for MSA again using ion chromatography and ESI/MS/MS.

149 **2.3 Calculation of anthropogenic Pb, non sea-salt S, and Br enrichment**

150 The Pb derived from anthropogenic sources (exPb) was calculated as the difference between total lead
151 measure in the ice core, $[Pb]_{obs}$, and that from dust sources. The Pb from dust was calculated as a
152 fraction of the dust proxy cerium, ($[Ce]_{obs}$).

$$\text{exPb} = [\text{Pb}]_{\text{obs}} - [\text{Ce}]_{\text{obs}} \times \left(\frac{[\text{Pb}]}{[\text{Ce}]} \right)_{\text{dust}} \quad (1)$$

Where the relative amount of Pb in dust, $([\text{Pb}]/[\text{Ce}]_{\text{dust}})$, has the constant mass ratio of 0.20588 (Bowen, 1979).

Similarly the amount of non-sea salt sulfur (nssS) was calculated relative to the sea-salt sodium, ssNa:

$$\text{nssS} = [\text{S}]_{\text{obs}} - [\text{ssNa}] \times \left(\frac{[\text{SO}_4^{2-}]}{[\text{Na}]} \right)_{\text{seawater}} \quad (2)$$

Where the amount of sulfur relative to Na in sea-water, $([\text{SO}_4^{2-}]/[\text{Na}]_{\text{seawater}})$ has the constant mass ratio of 0.252 (Millero, 1974). ssNa was calculated by comparison with calcium as both have sea salt and dust origins (Röthlisberger et al., 2002):

$$\text{ssNa} = \frac{[\text{Na}_{\text{obs}}] \times R_t - [\text{Ca}_{\text{obs}}]}{[R_t - R_m]} \quad (3)$$

Where R_t and R_m are the Ca/Na mean crustal and mean marine mass ratios of 1.78 and 0.038, respectively, (Millero, 1974).

Bromine enrichment factors relative to sea water concentrations were calculated using the following:

$$\text{enrBr}(\text{Na}) = \left(\frac{[\text{Br}]}{[\text{Na}]} \right)_{\text{obs}} / \left(\frac{[\text{Br}]}{[\text{Na}]} \right)_{\text{seawater}} \quad (4)$$

where the $([\text{Br}]/[\text{Na}]_{\text{seawater}})$ mass ratio is 0.00623 (Millero, 1974).

2.4 Air mass back trajectories

To identify the likely sea ice source regions of MSA and Br deposited at the ice core sites, we perform 10 day air mass back trajectories of boundary layer air masses from each ice core site using the GDAS1 archive dataset in the Hysplit4 software (Draxler and Hess, 1998). The starting height of the back trajectories was 500 m to ensure that the monitored air masses travelled close enough to the surface at the ice core site to potentially deposit aerosols. The vertical velocity field was taken from the

177 meteorological data files. Air mass back trajectories were started every 12 hours and allowed to travel
178 for 10 days (total number of trajectories hours = 14400 hours per month). The number of hours that the
179 trajectories spent in a 2°x2° degree grid was summed over all of the trajectories for that month between
180 the years 2005-2013. Previous work showed that the rapid advection of MBL air was the likely source
181 of reactive halogens at Summit (Sjostedt et al., 2007).

182 **2.5 Sea Ice Correlation mapping**

183 In order to assess the relationships between sea ice conditions and ice core chemistry, correlation maps
184 were generated between annual MSA concentrations and monthly sea ice using the HadISST1 ICE
185 dataset at 1° latitude-longitude monthly resolution (Rayner, 2003). Pre-1979 sea ice datasets were
186 interpolated from sea ice extent maps compiled by Walsh (1978) which incorporate a variety of
187 empirical observations. The data were later bias corrected using modern satellite data (Rayner, 2003).
188 Correlations were performed separately for the satellite period (1979-2012) and for the extended record
189 (1900-2012), excluding the period 1940-1952 when the record has no variability due to scarcity of data
190 (Rayner, 2003). Because strong DMS emissions occur in marginal sea ice zones (Sharma et al., 2012),
191 we considered both sea ice concentration (SIC) and the area of open water in the sea ice pack (OWIP)
192 which represents the size of the marginal sea ice zone. OWIP is defined as the difference between sea
193 ice area (calculated from sea ice concentration over the area of the grid cell) and sea ice extent (NSIDC).
194 A SIC of 15% was used as the threshold for a grid cell to contribute to sea ice extent. The area of OWIP
195 was calculated within the coastal areas as defined by the results of the air mass back trajectories (Sect.
196 3.4).

197 Outliers were removed from the MSA time series (see Fig. 2) before the correlations were performed.
198 The outliers were removed using the technique described by Sigl (2013) for identifying volcanic signals
199 using a 25 year running average filter. Correlations were performed on an annual rather than seasonal
200 basis because the seasonality of ice core MSA is distorted due to post-depositional migration of MSA
201 signal at depth in the snow pack (Mulvaney et al., 1992) (Fig. 3, S1).

202 203 **3 Results**

204 **3.1 Bromine**

205 Ice core measurements of bromine at Summit and Tunu covering the period 1750-2010 are shown in
206 Fig. 2. Ice core Br levels at each site were stable until ~1820 at Summit and ~1840 at Tunu when they

207 both decreased by ~ 1 nM, establishing a new baseline that was stable until the mid 1900s. Both ice cores
208 also show a Br peak in the late 20th century. The concentration values and the timing of inflections in
209 concentrations were determined by a 3 step linear regression of the data set. The analysis was performed
210 by simultaneous linear least squares fitting of 3 straight lines joined by ‘inflection points’ to the data
211 set. The variables of the fitting procedure were the slopes and intercepts of each line as well as the x-
212 axis locations at which the total function switched from one linear section to the next (the inflection
213 points). Initial guess values were supplied for each variable to help the fitting procedure reach
214 reasonable values. A summary of the regression results can be found in Table S1.

215 Sea-salt transport onto the Greenland ice sheet occurs predominantly during winter. Historically the
216 winter-time sea-salt maximum was believed to be due to increased cyclonic activity over the open
217 oceans (Fischer and Wagenbach, 1996) though more contemporary studies show that blowing snow
218 from the surface of sea-ice may be a significant source (Rankin et al., 2002; Xu et al., 2013; Yang et al.,
219 2008, 2010). At Summit, a winter-time maximum is observed in the most abundant sea salts, Na and Cl
220 (Fig. 3). Bromine also shows a significant winter-time signal, however the annual maximum appears in
221 mid-summer - at concentrations $\sim 70\%$ above winter levels (Fig. 3a). Comparison with Br measured in
222 weekly surface snow samples collected from Summit (from 2007-2013; GEOSummit project) confirms
223 that this summer signal is real and not a result of post-depositional modification of seasonality of the
224 bromine signal (Fig. S2). The results from that study confirm that total Br concentrations peak in
225 summer on the ice sheet closely following the Br cycle observed in the Summit-2010 ice core. In
226 addition to the comparison with the Geosummit data, in the ice cores studied here there are routinely
227 more than 10 measurements made within a yearly layer of snow giving confidence to the allocation of
228 a summer maximum in bromine at Summit. Analysis of the annual cycle of bromine in the Tunu ice
229 core also shows a summer maximum when averaged over the entire ice core time series but with
230 significantly larger error than observed at Summit. The timing of this peak suggests a predominant
231 summer-time deposition of bromine that dwarfs that from winter sea salt sources.

232 The shape of the annual bromine cycle does change slightly over the course of the Summit record (see
233 Fig. 3). Starting in the early 1900s the annual bromine cycle slowly becomes broader. A slight shift in
234 the maximum from a solely summer peak in the preindustrial era towards a broad summer-spring peak
235 by 1970 is observed (Fig. 3 lower plot). Comparison with the sea salt tracer, sodium, which does not
236 undergo the large temporal shift and broadening of its seasonal cycle shows that this change in bromine
237 seasonality is not linked to changes in production or transport of sea-salt aerosols or even dating
238 uncertainties in the ice core but perhaps the introduction of an additional, smaller bromine source in the
239 spring-time during the industrial era.

240 Both ice cores show a predominantly positive Br enrichment throughout the year (Fig. S3, S4) relative
241 to both sea salt elements chlorine and sodium. This enrichment reaches a maximum in mid to late
242 summer at Summit (Fig. 3). We assume that this enrichment reflects Br enrichment in the aerosol
243 transporting Br to the ice sheet. In a comprehensive review of global aerosol Br measurements, Sander
244 et al. (2003) concluded that in general, aerosols which showed positive Br enrichment factors were of
245 sub-micrometer size. These small aerosols can travel further (lifetimes of around 5-10 days) and due to
246 their larger surface/volume ratio may experience more atmospheric processing than larger aerosols,
247 resulting in the positive enrichment. However, post-depositional reduction of the bromine concentration
248 is a possibility during the summer months due to photolytic processes at the snow surface. This may be
249 the cause of the noisiness of the bromine signal within the lower accumulation, Tunu core. However,
250 the increased snow accumulation that occurs during the summer months in both central and northern
251 Greenland (Chen et al., 1997) should act minimise these bromine depleting effects driven by increased
252 insolation in summer and indeed Weller (2004) has shown that accumulation rates of this size are large
253 enough to prevent the post-deposition loss of other species such as nitrate and MSA.

254 Both sites also show a (small) positive enrichment of chlorine relative to sodium, which is amplified at
255 small sodium concentrations. Chlorine containing aerosols are expected to undergo similar chemical
256 processing to bromine containing aerosols but the enrichment factors of bromine (relative to sodium)
257 are much larger which is likely due to the high solubility of bromine species such as HBr (Sander et al.,
258 2003) . Alternatively, the chlorine enrichment could be interpreted as a sodium depletion of the aerosols
259 particularly in those of small diameter where both concentrations are low; this would amplify the
260 bromine enrichment (relative to sodium) but would not explain the bromine enrichment relative to
261 chlorine. It is likely that both halogens undergo some degree of enrichment and the sodium undergoes
262 some depletion in the aerosols though it is difficult to determine this from the data.

263 A summer-time maximum in Br enrichment was also observed by Spolaor (2014) in a short segments
264 of Antarctic Law Dome ice core as well as two Arctic ice cores. Spolaor et al. believe that the main
265 source of the inorganic bromine originated from spring-time bromine explosion events above sea ice
266 and the summer-time maximum could possibly be an indication of lag-time between bromine containing
267 particles becoming airborne and their deposition. Further investigation is needed to definitively establish
268 the seasonality of bromine deposition at the poles. However the results of the Arctic ice cores studied
269 here suggest that the summer maximum in bromine deposition is indeed real.

270 In the Tunu ice core, 11% of the monthly bromine enrichment measurements relative to Na were
271 negative (less than the Br/Na seawater ratio, Fig. S3) and 12% were negative relative to Cl. It is possible

272 that the negative enrichment values observed in the Tunu ice core are therefore a result of larger aerosols
273 (> micrometer) reaching the site due to its proximity to the coast (and thus the likely sea ice aerosol
274 source region) in comparison to Summit.

275 **3.2 MSA**

276 The Summit-2010 MSA record (Fig. 2) replicates that measured by Legrand in 1993 (Legrand et al.,
277 1997) and extends it an additional 17 years (see Fig. S5). The mean Summit-2010 MSA measurements
278 over the period 1984-1992 (2.0 ± 0.7 (1σ) ppb) also compare well with the results of the sub-annually
279 sampled Summit snow pit study performed by Jaffrezo et al., (1994); 2.1 ± 1.8 (1σ) ppb. Both the Legrand
280 and Jaffrezo studies measured MSA using ion chromatography of discretely sampled snow and ice. The
281 similarity between the Summit-2010 measurements and the results of these studies demonstrates that
282 the new, continuous technique is able to achieve a comparable accuracy in MSA measured
283 concentrations to the traditional, discrete technique. It also demonstrates that negligible amounts of
284 MSA are being lost by using the continuous melt method.

285 The Tunu measurements represent the first MSA profile at this location. Replicate measurements of the
286 entire Tunu ice core were performed with the on-line, continuous technique by melting a secondary
287 stick of ice cut from the original Tunu ice core. The replicate measurements closely followed the original
288 MSA measurements demonstrating the reproducibility, stability and high precision of the continuous
289 MSA technique (Fig. S6). The Tunu MSA record was also reproduced using discrete samples collected
290 from the CFA system (Fig. S7).

291 At Summit, MSA concentrations averaged 48 nM in the late 18th century, compared with just 27 nM at
292 Tunu. From 1878-1930 MSA concentrations at Summit plateaued at 36 nM after which they began to
293 drop rapidly, at a rate of 0.27 nM/year, reaching 18 nM by 2000 C.E.. Large fluctuations in the MSA
294 record after this time make it difficult to assess the most recent trend in Summit MSA concentrations.
295 MSA concentrations in the Tunu core showed a similar temporal variability to those in the Summit
296 record, and until the mid-20th century, were consistently lower in magnitude. MSA concentrations only
297 began to decline consistently at Tunu after 1984, almost 50 years after the rapid decline observed in the
298 Summit record. After 2000 C.E., large fluctuations in concentration were again observed making the
299 modern-day trend in MSA concentration at Tunu difficult to establish.

300 Comparison with the total sulfur record (Fig. 4) reveals that during the preindustrial period, MSA
301 contributes to ~12% and ~ 7% of the total sulfur signal at Summit and Tunu, respectively, compared
302 with < 2% at the height of industrial period (1970 C.E.) at both sites.

303 The low frequency, preindustrial trend in MSA concentrations seen in these ice core records closely
304 follows that of bromine; particularly distinct is the decrease in both MSA and bromine at both sites in
305 the early to mid 1800s (Tables S1 and S2). In the 1900s, however, both sites show a divergence between
306 the MSA and Br records—as MSA begins to decline, Br concentrations increase.

307 A dramatic shift in the ‘timing’ of the annual MSA maximum in Summit-2010 ice core is illustrated in
308 Figs. 3c and S1. The signal shifts gradually and continuously along the length of the the entire Summit-
309 2010 record from a spring to winter maximum (Fig. S1). This phenomenon has previously been
310 observed in several Antarctic ice cores and has been attributed to post-depositional migration within the
311 ice due to salt gradients (Mulvaney et al., 1992; Weller, 2004). At very low accumulation ice core sites
312 post-depositional loss of MSA (and nitrate) must also be considered. Extrapolation of data collected by
313 Weller (2004) from a series of East Antarctic ice cores predicts that sites with annual average
314 accumulations of greater than $105 \text{ kg m}^{-1} \text{ yr}^{-1}$ (0.105 m yr^{-1}) will not show post-depositional loss of
315 MSA (or nitrate). Both ice cores in this study have sufficient average annual accumulation that post-
316 depositional loss of MSA (and nitrate) is predicted to be negligible and so is not discussed further.

317 **3.3 Acidic Species**

318 In winter, with the collapse of the polar vortex, polluted air masses enter the Arctic region as the
319 phenomenon known as the Arctic haze (Barrie et al., 1981; Li and Barrie, 1993). SO_2 and NO_x from the
320 haze are adsorbed onto aerosols or deposited directly on the ice/snow and oxidised to sulfuric (H_2SO_4)
321 and nitric acid (HNO_3). There are also natural sources of SO_2 (biomass burning, volcanic eruptions,
322 oceans (Li and Barrie, 1993; McConnell et al., 2007; Sigl et al., 2013) and NO_x (microbial activity in
323 soils, biomass burning, lightning discharges (Vestreng et al., 2009) as well as other snow/ice acidifiers
324 including MSA, hydrogen chloride and organic acids released from biogenic or biomass burning sources
325 (Pasteris et al., 2012).

326 The annual cycle for nitrate (NO_3^-) is shown in Fig. 3d. Before 1900 C.E. the nitrate shows a seasonal
327 maximum in late summer/early fall after which the maximum shifts to late spring/early summer.
328 Although there are biological sources of nitrate in the ice core aerosol source regions, in a recent study
329 focused on the NO_3^- and $\delta^{15}N - NO_3^-$ record in the Summit-2010 ice core, Chellman et al. (2016)
330 concluded that the preindustrial (1790-1812 C.E.) NO_3^- seasonal cycle was driven by biomass burning
331 emissions. However, in the modern era (1930-2002 C.E.) oil-burning emissions became the dominant
332 source of NO_3^- in the snow-pack. The change in the dominant NO_3^- source due to industrialisation is the
333 cause of the shift in timing of the seasonal cycle.

334 Total snow acidity was stable at both sites from 1750 through to ~1900 C.E. except for sporadic, short-
335 lived spikes due to volcanic eruptions. The average preindustrial acidity was the same at both sites (~1.8
336 μM). Both records also show two distinct maxima in acidity centred on 1920 and 1970 C.E. (Fig. 4)
337 with Tunu displaying higher acidity than Summit over the entire industrial period. Overlaid with the
338 acidity is the total sulfur (S) record for both ice cores. The high correlation between the acidity and S
339 records illustrates that the sulfur species are the dominant natural and anthropogenic acidic species in
340 the ice cores. The trend in acidity closely follows the global SO_2 emissions with maxima from coal
341 (~1920 C.E.) and coal plus petroleum combustion (~1970 C.E.), respectively (Smith et al., 2011). After
342 1970 the records of acidity and S deviate. This deviation can be attributed to the presence of nitric acid
343 that remains at a relatively high concentration in the late 20th century whilst sulfur species reduce in
344 concentration (Fig. 4).

345 NO_3^- concentrations show no trend during the preindustrial era in either ice core records, averaging
346 $1.1(\pm 0.02) \mu\text{M}$ and $1.3(\pm 0.03) \mu\text{M}$ for Summit and Tunu, respectively. The higher signal-to-noise ratio
347 in the Summit-2010 record reveals a small peak in NO_3^- concentrations centred on ~1910. The Tunu
348 record also shows elevated NO_3^- concentrations over this period. However the large variability in the
349 signal makes it difficult to establish a higher resolution temporal trend. Both records clearly show a
350 large increase in NO_3^- after 1950, peaking in ~1990 and followed by a general decreasing trend with the
351 average NO_3^- levels still double that of preindustrial concentrations: $2.1 \mu\text{M}$ and $2.3 \mu\text{M}$ at Summit and
352 Tunu, respectively.

353 The nitrate records from both sites follow the trend in northern hemisphere NO_x emissions with a peak
354 in ~1910 and 1990 C.E.– a result of emissions from increases in both Northern Hemisphere fertilizer
355 usage and biomass and fossil fuel combustion (Felix and Elliott, 2013).

356 **3.4 Air mass back trajectories**

357 Air mass back trajectory results demonstrate that air masses reaching the Summit-2010 site between
358 March and July originate primarily from the South/South-East of the ice core site (Fig. 5a). Previous
359 back trajectory analyses by Kahl *et al.* (1997) also linked individual spikes in their Summit MSA record
360 to air masses that had passed over this same region of coast (SE Greenland) within the previous 1-3
361 days. Similar back trajectories were calculated for Summit-2010 up to heights of 500 and 10,000m (total
362 column trajectory, Fig. 5a, S8a) illustrating that air masses that travel in the free troposphere and lower
363 troposphere follow similar back trajectories and likely share the same source regions.

364 The results for Tunu indicate that air masses arrive primarily from the west coast of Greenland, passing
365 over the Baffin Bay area, but there is also significant contribution from both the SE and NE (in May)
366 coastal areas (Fig. 5b, S8b). Of these two secondary areas it is likely that aerosols transported from the
367 NE would have a greater influence on the ice core concentrations due to proximity to the ice core site.
368 Aerosol deposited at Tunu therefore represents a mixture of source regions, but are likely dominated by
369 the NW Greenland, Baffin Bay coastal region.

370 **3.5 MSA - Sea Ice correlations**

371 Locations which showed a sea ice concentration (SIC) variability greater than 10% (the average
372 estimated range of uncertainty in the satellite measurements) and have a significant correlation to MSA
373 (t-test, $p < 0.05$) are displayed in Figs S9 and S10 for the months of March-July. A greater weight must
374 be placed on the post-1979 sea ice concentration maps as these were derived from passive microwave
375 satellite data and, where available, operational ice chart data. The likely air mass source regions, as
376 defined by the results of the air mass back trajectories, are indicated by the black bordered regions.
377 Within these areas there is generally a negative correlation between SIC and MSA, particularly in the
378 spring months and only small patches that show large correlation (>0.4). The large areas of positive
379 correlation along the east coast and in the western Barents Sea are striking for the Summit-2010 record,
380 however, these areas are outside of the defined air mass source region and thus are unlikely to be
381 contributing to the ice core aerosol records. The positive correlation is likely an artefact of the negative
382 autocorrelation between sea ice conditions in this region and the SE coast source region (Fig. S11).

383 The effect of the estimated error in dating of the MSA records on the SIC correlation maps is explored
384 in Fig. S12. By shifting the dating of the MSA records to either extreme of the dating error estimate and
385 replotting the SIC correlation plots it is clear the error in the dating of the MSA records does not affect
386 the sign of the correlations displayed on the maps but can have an affect on the magnitude of the
387 correlation found in different locations. This is likely a result of the peaks in the MSA record being
388 shifted in or out of temporal coherence with peaks in SIC at the different locations.

389 Over the period 1900-2010 C.E. highly significant correlation (t-test, $p < 0.001$) is found between the
390 annual ice core MSA and the amount of open water in the ice pack (OWIP, representing the area of the
391 marginal sea ice zone, Figs. 6a and 7a; lower plots) in these aerosol source areas. For both ice cores the
392 source region OWIP trend is followed by the MSA. In the Summit-2010 ice core the highest correlation
393 between annual MSA and monthly OWIP occurs in May ($r = 0.58$, $p < 0.001$) though the following months
394 through to July all show highly significant correlations (July $r = 0.53$, $p < 0.001$). For comparison, the May

395 SIC correlation map is also shown as the upper plots in Figs. 6a. Figs. 3f and S13 demonstrate that this
396 time period (May-July) corresponds to the peak and then rapid decline in the amount of annual OWIP
397 within the Summit-2010 aerosol source area because of the decreasing extent of sea ice. Rapid loss of
398 sea ice reveals areas of biological activity previously capped by the ice allowing surface-atmosphere
399 exchange of DMS, resulting in the seasonal peak in atmospheric MSA correlation with the peak in the
400 area of OWIP.

401 At Tunu the highest correlation over the 1900-2012 C.E. period is found between annual MSA and
402 annual OWIP ($r=0.59$, $p<0.001$), though the July OWIP shows the highest monthly correlation and is
403 also highly significant ($r=0.41$, $P<0.002$). For comparison, the July SIC correlation map is also shown
404 as the upper plots in Figs. 7a. Due to the more northerly location of the Tunu aerosol source region, the
405 sea ice pack in this region is generally less fractured and break-up occurs later in the year, with a sharp
406 peak in OWIP occurring in July (Fig. S13). The higher stability of the ice pack throughout the year
407 compared to that in the Summit-2010 source region is the likely reason the Tunu MSA shows highest
408 correlation with the annual average of the OWIP. However, like Summit-2010 the highest monthly
409 OWIP correlation occurs between the annual MSA and the timing of the maximum in annual OWIP
410 (July).

411 Over the shorter, satellite era (1979–2012 C.E.) again Tunu shows strongest correlation between annual
412 MSA and annual OWIP though at a much lower significance ($r=0.32$, $p<0.05$), and the highest monthly
413 correlation occurs in March ($r=0.2$, $p<0.1$) albeit with low significance. The significance of the Tunu
414 correlation over this period can be dramatically increased (annual OWIP $r=0.54$; $p<0.001$, March OWIP
415 $r=0.63$, $p<0.001$) if the closer, secondary aerosol source region (NE Greenland, 80° – 73° N, 20° – 0° W)
416 is assumed to also influence the site in equal proportion. March corresponds to the timing of increased
417 insolation and thus the rapid increase in ice algal production (Leu et al., 2015). The shift from a July to
418 March peak in the correlation of OWIP with annual Tunu MSA may be a result of the reduced overall
419 SIE (and thus OWIP) influencing the timing of MSA production. Unfortunately, the post-depositional
420 migration of the MSA signal within the ice cores masks any evidence of true seasonal MSA shifts.
421 Summit-2010 also shows a much less significant monthly OWIP correlation with the annual MSA signal
422 over this time period, with the most significant correlation again occurring in March ($r=0.4$, $p<0.02$).
423 The greater significance of both the SIC-MSA and OWIP-MSA correlations at both sites over the longer
424 time period is likely a result of the averaging of any MSA production or transport variability as well as
425 the dominance of the low frequency variability of both time series on the overall correlation.

426 **3.6 MSA and bromine relationship**

427 In an era where climate is driven by only natural forcings, chemical species that share a common source
428 should show broadly consistent variability. This is evident in the preindustrial section of both ice core
429 records where the relationship between MSA and Br (monitored as Br/MSA) remains constant over the
430 entire period (Fig. 4) despite individual records going through step function changes. Using a 25 year
431 running average on all records, the correlation between MSA and Br over the preindustrial period was
432 calculated as: Summit-2010: $r=0.282$ ($p=0.0008$); Tunu: $r= 0.298$ ($p = 0.0004$), $n= 138$. After ~1930
433 C.E., relative increases in Br concentrations cause the Br/MSA ratio to increase above the stable
434 preindustrial levels by more than 160%, reaching a peak in ~2000 C.E. at both sites.

435 Bromine in excess of what is expected from a purely sea ice source (non sea ice bromine, nsiBr) was
436 calculated by comparison to the other sea ice proxy, MSA. A linear regression of MSA versus Br was
437 performed with the preindustrial data (1750-1880 C.E.) to establish the relationship between the two
438 proxies during an era free of anthropogenic forcing (Figure S14a,b). This relationship was then
439 extrapolated into the period after 1880 C.E. in order to estimate the amount of bromine sourced only
440 from sea ice sources during the industrial era. The MSA record was smoothed with a 9th order
441 polynomial function before being used in the extrapolation to reduce the noise in the resultant record
442 whilst maintaining the low frequency trends (Figure S14c,d). nsiBr is thus the difference between the
443 total bromine measured and the calculated, natural sea ice bromine (Figs. 8 and S14e,f); in contrast to
444 Br_{exc} defined by Spolaor (2016) as the amount of bromine in excess of the Br/Na seawater ratio.

445 An estimate of the nsiBr is shown in Figs. 6,7 and 8. By definition, nsiBr is essentially constant during
446 the preindustrial period, but during the industrial period nsiBr peaks, reaching a broad maximum
447 between 1980-2000 C.E. of ~3.4nM and 1.9nM at Summit and Tunu, respectively.

448 **4 Discussion**

449 The significant correlation between variability of marginal sea ice zone (OWIP) area within the
450 identified source regions and the MSA records suggests that MSA records can be used as a proxy for
451 modern sea ice conditions in these areas. North Atlantic Oscillation (NAO) proxy records developed in
452 Greenland ice core records (Appenzeller et al., 1998) suggest that although the northern hemisphere
453 climate phenomenon has shown variability over the past 200 years, its effect is damped in Northern
454 Greenland (Appenzeller et al., 1998; Weißbach et al., 2015) so we can assume that no major changes in
455 atmospheric circulation patterns have occurred to change the source regions for the marine aerosols
456 between the preindustrial and industrial periods. If this assumption is true, our identification of MSA as
457 a sea ice proxy (specifically a marginal sea ice zone proxy) may be valid for time periods both before

458 and after 1850 at each ice core site.

459 The MSA records reveal that after 1820 C.E. a gradual decline in sea ice occurred along the southern
460 Greenland coast (reflected in the Summit-2010 core) and that this decline in sea ice did not extend
461 significantly to the most northern Greenland coastline (reflected in the minimal change in Tunu MSA
462 during this period). It is not unexpected that the Summit-2010 record would show the most dramatic
463 changes in sea ice since we have demonstrated that the Summit sea ice proxy (MSA) is sourced from
464 the south-east Greenland coast – an area sensitive to climate changes as it is primarily covered by young,
465 fragile sea ice. The timing of the sea ice decline is coincident with the end of the Little Ice Age, identified
466 from $\delta^{18}\text{O}$ ice core records as spanning the period 1420-1850 C.E. in Greenland (Weißbach et al., 2015).
467 The dramatic dip in sea ice reflected in both the Tunu MSA and Br records at 1830 C.E. (and also seen
468 less dramatically in Summit) also appears in the multi-proxy reconstruction of sea ice extent in the
469 Western Nordic Seas performed by Macias Fauria et. al. (2010). This may be evidence of a 1830 C.E.
470 sea ice decline event isolated to the east Greenland coast as the ice core records do not replicate the
471 other dramatic, early 20th century fluctuations observed in the latter part of the Western Nordic Seas
472 reconstruction.

473 From the ice core records it appears that the greatest decline in Greenland sea ice began in the mid 20th
474 century, dropping to levels that are unprecedented in the last 200 years. This decline is observed along
475 the entirety of the Greenland coast. Sea ice declined first around the southern coast (from 1930 C.E.,
476 reflected in Summit-2010) followed 54 years later by the more northern coastline (reflected in the Tunu
477 record, see infection timings in Table S1). This sea ice decline is coincident with the sustained increase
478 in greenhouse gases which has been identified as the major climate forcing and driver of increased
479 global temperatures during the 20th century (Mann et al., 1998) and follows the same general trend in
480 Arctic wide sea ice extent observed by Kinnard (2008).

481 Bromine (more specifically bromine enrichment (Spolaor et al., 2014) and bromine excess (Spolaor et
482 al., 2016)) has also been suggested as a possible proxy for sea ice conditions, however the timing of the
483 largest bromine aerosol deposition, in summer, does not coincide with the largest growth or extent of
484 new sea ice. Sea ice begins to increase only at the end of summer as the fractures in the ice cover are
485 re-laminated and the ice edge begins to advance southward (see Fig. 3f). Fig. S4 compares the record
486 of total bromine and bromine enrichment (calculated relative to sodium, enrBr(Na)) from the Summit-
487 2010 ice core. The major discrepancies between the two records occur when the total sodium signal has
488 sharp maxima causing dips in the enrBr(Na) record in ~1954 and 1990 C.E. and the magnitude of the
489 low frequency variability in enrBr(Na) is not as great as in the total bromine record. This is also

490 demonstrated in figs. 6 and 7 where the enrBr(Na) records are compared with the OWIP records. Whilst
491 both series share high frequency temporal features, over the longer term (1900-2010) the low frequency
492 trend is dramatically different. We are not discounting enrBr(Na) as a viable proxy for sea ice
493 conditions, however the use of Na to try and extract the pure sea water component of the Br is
494 complicated by the fact that a lot of Na comes from the sea ice surface as well as from the open ocean.
495 Na itself has been used as a sea ice proxy in several prominent studies (Wais Divide Project Memembers,
496 2013; Wolff et al., 2003) because, like Br, Na is incorporated into the snow on the surface of the sea ice
497 and can be subsequently blown aloft to produce the atmospheric Na signal seen in the ice core. In
498 addition, the Na concentration is fractioned upon the formation of the ice when mirabilite (Na_2SO_4) is
499 precipitated out of the brine solution at -8°C (Abbatt et al., 2012).

500 The calculated, non-sea ice bromine records (nsiBr) for both ice cores are shown in figs. 6 and 7. Like
501 the enrBr(Na) records, the nsiBr records share some of the high frequency features of the OWIP records,
502 however there is no significant correlation between nsiBr and the selected OWIP records over the short
503 time period. This supports the supposition that the nsiBr record is indeed an extraction of the non-sea
504 ice component of bromine from the total bromine record. Over the longer time period there is a
505 significant negative correlation between OWIP and nsiBr at both sites (Summit-2010: $r=-0.7$, $p<0.001$,
506 Tunu: $r=-0.22$, $p<0.02$). This result is likely an artifact of the positive correlation from the MSA records
507 used to generate the nsiBr records.

508 So what is the summer-time source of bromine? What is the cause of the increase in spring-time bromine
509 explosion events in the industrial era? (see Fig. 3, lower panel) and why does the bromine record deviate
510 from the sea ice proxy record (MSA) around the same time? Possible sources of bromine and the factors
511 which may effect the resultant bromine deposition flux are discussed below.

512

513 **4.1 Alternate sources of bromine**

514 **4.1.1 Combustion of coal**

515 Bromine is present in coal (Bowen, 1979; Sturges and Harrison, 1986) and coal burning is therefore a
516 potential source of increased bromine deposition on the Greenland ice sheet over the period 1860-1940
517 (McConnell and Edwards, 2008). McConnell et al. (2007) demonstrated that pollution from the
518 Northern American coal burning era was deposited all over Greenland leaving as its fingerprint large
519 amounts of black carbon and toxic heavy metals. Sturges (1986) measured the relative concentrations

520 of Br and Pb in particulates emitted from the stacks of coal fired power stations and found a molar ratio
521 (Br:Pb) ranging between 0.36-0.67:1. Figure 8 illustrates that at both Summit and Tunu the exPb (lead
522 not from dust sources) preserved in the ice cores over the coal burning era (~1920) was less than 1nM.
523 This concentration implies that the upper limit to the amount of bromine deposited from coal
524 combustion would be 0.67nM (assuming no loss of bromine from the particulates during transportation).
525 This is an insignificant amount compared to the total Br signal preserved in the ice at this time. Coal
526 combustion is not the major cause of the elevated industrial Br concentration.

527 **4.1.2 Leaded Gasoline**

528 The largest global, historical, anthropogenic source of bromine is thought to be the combustion of leaded
529 gasoline. Large quantities of 1,2-dibromoethane (DBE) were added to leaded fuel as a scavenger for Pb
530 preventing lead oxide deposition by converting it to volatile lead bromide salts as well as CH_3Br (Berg
531 et al., 1983; Nriagu, 1990; Oudijk, 2010). In 1925 C.E. gasoline had a Br:Pb molar ratio of 2:1 in a
532 formulation which is now called “aviation fluid”. The Br:Pb molar ratio was reduced to 1:1 in the 1940s
533 except in places such as the Soviet Union which continued to use “aviation fluid” for motor gasoline
534 (Thomas et al., 1997). Although the consumption of leaded gasoline has been well documented,
535 particularly in North America, the estimates of the emissions of bromine compounds from the
536 combustion process are still unclear. Estimates of the amount of DBE that is converted into gaseous
537 CH_3Br range from 0.1% to 25% (Bertram and Kolowich, 2000) and direct measurements of exhaust
538 fumes across NW England found a Br:Pb ratio of between (0.65-0.8):1 in the airborne particulates
539 (Sturges and Harrison, 1986).

540 The ratio of Br:Pb in the gasoline formulae can therefore be used only as an upper limit to predict the
541 Br:Pb ratio in gasoline combustion aerosols transported to the ice core sites. Figure 8 shows a
542 comparison between nsiBr and exPb measured in each ice core. Also illustrated is the upper limit of the
543 amount of bromine expected from gasoline sources assuming the 2:1 Br:Pb ratio for aviation gasoline
544 over the whole leaded gasoline era. World-wide leaded gasoline emissions were estimated to have
545 peaked in 1970 C.E. (Thomas et al., 1997)—an assumption that is supported by the observed timing of
546 the exPb maximum observed in both ice cores. Whilst it is likely that leaded fuel contributed to the
547 increased bromine observed between 1925 and 1970, it is clear that it was not the only contributor to
548 the nsiBr record, particularly after 1970 when the nsiBr record continues to rise despite a worldwide
549 decline in leaded fuel consumption. The disparity between the exPb and nsiBr records suggests the
550 driving force for the enhanced emission of Br was still active and increasing after 1970.

4.1.3 Seasonal salinity changes

Younger sea ice surfaces such as frost flowers, new and 1st year sea ice have a higher salinity and thus have higher bromine concentrations than older sea ice surfaces (Hunke et al., 2011). The salinity of sea ice is at its maximum at the start of the winter season after which surface salinity slowly diminishes due to gravitational draining (Hunke et al., 2011). As summer approaches, ice continues to undergo desalination due to melting of surface snow which percolates through the ice (Hunke et al., 2011). Satellite observations that the BrO flux from the sea ice declines over summer (despite increasing insolation) is likely due to the combined reduction in young sea ice area and in ice salinity. Ocean surface salinity decreases in the summer due to the increased meteoric water flux and melting of desalinated sea ice. Salinity increases are therefore unlikely to be the sole cause of the nsiBr flux observed in the ice core records and the observed summer maximum in bromine.

4.1.4 Organic bromine species

Gaseous bromocarbons can be a source of inorganic bromine to the snow pack when they react with $\bullet\text{OH}$ or to a lesser extent with $\bullet\text{NO}_x$ or by photolysis (Kerkweg et al., 2008; WMO, 1995) to form the less reactive species HBr , BrNO_3 and HOBr . These species can then be washed out of the atmosphere and deposited on the snow surface due to their high solubility (Fan and Jacob, 1992; Sander et al., 1999; Yung et al., 1980).

The predominant source of gaseous bromine in the atmosphere is methyl bromide, CH_3Br (WMO, 2002). The major modern sources of CH_3Br are fumigation, biomass burning, leaded fuel combustion, coastal marshes, wetlands, rapeseed and the oceans (WMO, 2002). The ocean is also a major sink for CH_3Br , the temperature sensitive dissolution occurring through hydrolysis and chloride ion substitution to form bromide (WMO, 1995). $\sim 30\%$ of CH_3Br was from industrial emissions at the time of the global peak in the CH_3Br mixing ratio (1996-1998) (Montzka and Reimann, 2010). The timing of the massive increases in nsiBr seen at both ice cores sites coincides with the timing of maximum anthropogenic emissions of CH_3Br . However, the estimated 2.7 ppt increase in global tropospheric CH_3Br above preindustrial levels equates to only ~ 3.7 ppt (0.05nM) Br incorporated into the snow pack (assuming 100% conversion efficiency of CH_3Br in soluble Br species). This level is far less than the 2-5 nM increase in nsiBr observed in the ice cores during the industrial period.

Bromoform (CHBr_3) is emitted from vegetation such as marine phytoplankton and seaweed. It has the largest globe flux of all the bromocarbons (estimated at almost 5 times that of CH_3Br (Kerkweg et al., 2008). However, it is very short-lived (atmospheric lifetime of ~ 17 days (Ordóñez et al., 2012) and

582 thus is confined to the marine boundary layer. Inorganic bromine formed from the destruction of $CHBr_3$
583 would therefore be representative of only local sources of organic bromine. The biological seasonal
584 cycle maximises the production of $CHBr_3$ in summer and concentrations are greatly reduced but not
585 negligible in winter (tidal forcing also influences bromocarbon emission by allowing coastal algae to
586 dry-out (Kerkweg et al., 2008). The season of Arctic sea ice algae productivity is confined by limitations
587 in available sunlight and nutrients resulting in a mid-to-late spring maxima – depending upon site
588 location (Leu et al., 2015) – as is reflected in the seasonality of the MSA record. Direct transport of
589 bromine enriched aerosols from these algal sources to the ice core sites again cannot explain the summer
590 maximum of bromine observed in the ice. In addition to the incoherence of the seasonality of the
591 bromine ice core signal, to-date biogenic sources have been considered insignificant sources of bromine
592 in the Arctic marine boundary layer compared with the inorganic bromine source from sea salts
593 (Simpson et al., 2007).

594 **4.2 Cause of the spring-time increase in bromine flux**

595 **4.2.1 Bromine explosion events**

596 Spring is the time of ‘bromine explosion’ events above sea ice. Sea salt aerosols passing through these
597 BrO plumes can become enriched with bromine by adsorbing the gaseous species (Fan and Jacob, 1992;
598 Langendörfer et al., 1999; Lehrer et al., 1997; Moldanová and Ljungström, 2001; Sander et al., 2003).
599 Nghiem (2012) showed that these bromine rich air masses can then be elevated above the planetary
600 boundary layer and transported hundreds of kilometres inland. Increasing the frequency and duration of
601 the bromine explosion events would therefore likely increase the amount of bromine delivered to the
602 ice core sites during spring without influencing the total aerosol flux and thus explain the shift in the
603 bromine seasonal concentrations from a purely summer to a broad spring-summer maxima (Fig. 3).

604 Spring-time field studies at Ny Ålesund, Svalbard have shown positive correlation between atmospheric
605 filterable bromine species and elevated levels of sulfate and nitrate (Langendörfer et al., 1999; Lehrer
606 et al., 1997) suggesting that acidic, anthropogenic pollution may be the driver of the observed increases
607 in annual bromine enrichment during the industrial period and seasonal shift.

608 **4.2.2 Acidity effects on debromination**

609 In remote, relatively clean environments such as the Arctic, even small increases in acidity are thought
610 to affect the cycling of bromine in the snow pack (Finlayson-Pitts, 2003; Pratt et al., 2013; Sander et al.,

511 1999). In the laboratory, increasing the acidity of frozen (Abbatt et al., 2010) and liquid salt solutions
512 (Frinak and Abbatt, 2006; George and Anastasio, 2007) increased the yield of gas-phase Br_2 whilst at
513 the same time increasing the *solubility* of other bromine species, such as HBr . The uptake efficiency of
514 HBr by acidic sulfate aerosols, for example, is estimated at 80% compared to 30% for sea salt aerosols
515 (Parrella et al., 2012). Interestingly, Abbatt (1995) demonstrated that HBr is more than 100 times more
516 soluble in super-cooled sulfuric acid solutions than HCl . This may explain the cause of bromine
517 enrichment in the aerosol measured in the ice cores relative to the more abundant chlorine (Fig. S3).
518 The results of both the laboratory and field studies suggest that increasing snow/ice acidity in the Arctic
519 will likely enhance spring-time bromine explosion events above the sea ice whilst the increase in
520 solubility allows the termination products of the explosion to be transported away from the sites on the
521 surface of acidic aerosols. Increasing spring-time bromine aerosol concentrations would increase the
522 average annual bromine concentrations deposited on the ice sheet and could explain the nsiBr records
523 observed in both ice cores.

524 There are also significant periods over which the calculated nsiBr record shows negative values (e.g.
525 1815-1870 C.E. in Summit-2010 and 1860-1940 C.E. in Tunu). The negative values are a result of the
526 Total Br being less than that calculated by interpolation from the smoothed MSA record. Though the
527 sources of Br and MSA are linked – which is what provides the similarities between the general low
528 frequency trend of the two species, the atmospheric processing, transport and deposition of the two
529 species may be modified by different variables such as changes in atmospheric acidity, for example.
530 These variables cause the short term differences between the MSA and Total Br records preserved in
531 the ice so we believe it is not unreasonable to expect negative values in the calculated non-sea ice Br
532 record when the MSA and Total Br are close (essentially no nsiBr).

533 Figure 9 illustrates that of the two dominant acidic species preserved in the ice, HNO_3 (represented by
534 nitrate) shows the highest correlation to total bromine over sub-decadal time scales at both ice core sites.
535 Records were detrended with an 11 year running average before comparison to isolate the high
536 frequency components of each record. The bromine – sulfuric acid (represented by sulfate) correlation
537 is not significant. This is primarily because there is no bromine response to the dominant volcanic sulfate
538 spikes throughout the record. The large spikes in sulfate concentrations did not cause a depletion of
539 bromine preserved in the snowpack (Figure 9). This result might be expected if the increased acidity
540 caused more bromine to volatilize. These results suggest that HNO_3 is the most influential of the MBL
541 acidic species in the processing and transport of Br on aerosols in the MBL.

4.2.3 NO_x and links to bromine

The snow and atmospheric chemistries of bromine and nitrate (NO_3^-) are tightly linked. NO_3^- is one of the main sources of the •OH radical. The •OH radical can oxidize bromide salts and cause the release of gas-phase bromine species (Abbatt et al., 2010; Chu and Anastasio, 2005; George and Anastasio, 2007; Jacobi et al., 2014). Morin et al. (2008) observed that the majority of nitrate that is deposited to the snow surface is of the form $BrNO_3$ in coastal Arctic boundary layer. $BrNO_3$ forms by gas-phase reaction of BrO and NO_2 . $BrNO_3$ is quickly adsorbed back onto the snow and aerosol surfaces due to its high solubility. The heterogeneous hydrolysis of $BrNO_3$ to again release bromine species back into the gas-phase has also been observed (Parrella et al., 2012) and can occur both during sunlight hours as well as in the dark (Sander et al., 1999). However, the study of Thomas et al. (2012) into the cycling of NO_x and bromine species in the snowpack at Summit concluded that the presence of snow NO_3^- would suppress the emission of BrO from the snow pack and into the interstitial air.

In spring, when the greatest concentrations of BrO are observed over the sea ice the atmospheric concentrations of NO_x species is rising. After 1900 C.E. there was, on average, a 60% increase in spring NO_3^- concentrations observed in Summit-2010 ice core (Fig. 3d) which, as discussed in Sect. 4.2.1, if reflected in the concentration of acidic aerosols landing on the sea ice (specifically HNO_3 concentrations) would enhance the emission of BrO into the MBL. Satellite imagery shows that bromine in the form of BrO is confined primarily to the atmosphere above sea ice (Schönhardt et al., 2012; Wagner et al., 2001) but the presence of measurable bromine concentration hundreds of kilometres inland preserved in the ice cores demonstrates that the bromine must be transported inland, just not in the form of BrO . The reaction of atmospheric NO_2 with BrO can produce the highly soluble $BrNO_3$ which will preserve the bromine in the aerosol allowing it to be transported inland. If there are high NO_3^- concentrations at the deposition site this will aid in fixing the bromine into the snow pack. This is supported by the observation that NO_3^- snow pack concentrations reach a maximum in summer, coherent with bromine snow pack concentrations even though maximum Br emission from the sea ice occurs in spring. So it appears that NO_x in its different forms, as NO_2 , NO_3^- , HNO_3 , or $BrNO_3$ is intertwined with Br as it cycles between the gas and condensed phases and as it is transported from sea ice source to deposition site. Elevated levels of NO_x over the Arctic could thus be the cause of the deviation of the bromine record from the MSA, sea ice proxy record.

The high correlation between the preindustrial (1750-1850 C.E.) NO_3^- and Br records (Fig. 9) supports this observation of co-transport and sink of Br and NO_3^- into the snow pack, though the natural sources of each are distinctly different. In the industrial era the low frequency temporal profile of the total

574 bromine and nitrate records differ considerably, particularly at Summit (Fig. S15), apparently
575 questioning the tight relationship observed before 1850. However, the positive correlation between the
576 nitrate and the Br/MSA (Fig. 4) and nsiBr (Fig. 8) records is striking at both sites. The large relative
577 increase in bromine (compared with MSA) during the era of high NO_x pollution may point to a non-sea
578 ice source of bromine linked to nitrate emissions or simply an increased spring-time emission and
579 summer-time deposition of Br from sea ice sources.

580 Bromine and NO_x species shared a common source in the 20th century through the combustion of leaded
581 gasoline (Sect. 4.1.2). As discussed above, we observe that leaded fuel pollution reaching the Arctic
582 began to decline after 1970 in-line with reduced global consumption, but the amount of bromine in-
583 excess of natural sources (nsiBr) continued to increase – following the trends in NO_x pollution (Fig.
584 8a). The continued increase in NO_x despite the decline in leaded fuel combustion is attributed primarily
585 to biomass burning, soil emissions and unleaded fossil fuel combustion (Lamarque et al., 2013). As the
586 leaded fuel source of bromine began to decline, organic bromine pollutants continued to increase, as
587 was discussed in Sect. 4.1.4. This can only account for a small fraction of the observed Br. The
588 continued correlation between nitrate and nsiBr despite the decoupling of nitrate and bromine
589 anthropogenic sources after 1970, suggests that nitrate pollution is likely influencing the processing of
590 local, natural sources of bromine in the polar MBL, in effect increasing the mobility of the bromine and
591 thus its flux and preservation in the ice sheet.

592 **4.2.4 Consequences of nitrate driven increased bromine mobility in the Arctic**

593 Plumes of BrO emitted from sea ice regions have been linked to mercury deposition events which lead
594 to an increase in the bioavailability of toxic mercury species in polar waters (Parrella et al., 2012).
595 Increased spring-time mobilization of bromine from the sea ice induced by anthropogenic nitrate could
596 therefore increase the frequency and duration of these events and thus the mercury toxicity of the oceans.
597 Increased atmospheric bromine concentrations would also increase the frequency of ozone depletion
598 events (Simpson et al., 2007) thereby altering the oxidative chemistry of the polar MBL.

599 Whilst several studies have begun to explore bromine records from ice cores as a proxy for past sea ice
700 conditions, the results of this study demonstrate that in an era of massive increases in atmospheric acidity
701 the natural relationship between bromine and sea ice conditions can become distorted, precluding it
702 from being an effective modern-day Arctic sea ice proxy.

703

704 **5 Conclusion**

705 In this study we have shown that high resolution MSA measurements preserved in ice cores can be used
706 as a proxy for sea ice conditions (specifically the size of the marginal sea ice zone) along specific
707 sections of the Greenland coast. The MSA records show that sea ice began to decline at the end of the
708 LIA and again, more dramatically during the Industrial period. Also, unsurprisingly, the changes in sea
709 ice conditions in the northern sites have been less dramatic than along the southern coastline.
710 Comparison between the 260 year records of bromine and MSA presented in this study allow us to show
711 that in the preindustrial era bromine concentrations preserved in the Greenland ice sheet are also likely
712 linked to the local sea ice conditions. With the decline of sea ice in the modern era and the dramatic
713 increase in acidic pollutants reaching the Arctic the sea ice-bromine connection is distorted, precluding
714 it from being an effective, direct sea ice proxy during the industrial era. The introduction of *NOx*
715 pollution in particular, into the clean Arctic environment promotes mobilization of bromine from the
716 sea ice, which in turn increases the bromine enrichment of the sea salt aerosols, forcing more bromine
717 inland (particularly in spring) than would occur naturally. Nitrate has also been linked with the
718 mechanism for preservation of bromine in the snowpack. The summer-time maximum of nitrate may
719 therefore be responsible for the observed summer-time bromine maximum preserved in the ice cores.
720 Whilst Northern Hemisphere pollution may prevent bromine from being an effective modern-day sea
721 ice proxy in the Arctic, in Antarctica the anthropogenic flux of nitrate species is thought to be small in
722 comparison with natural sources (Wolff, 2013), leaving room for the possibility that bromine may still
723 be an effective proxy for local Antarctic sea ice conditions and for preindustrial sea ice reconstructions.

724

725

726 **Author contribution**

727 Manuscript written and data analysis performed by O.J.M with expert editing by E.S.. Ice cores supplied
728 by J.R.M.. Tunu ice core was collected and processed by O.J.M, J.R.M., N.J.C, M.S., R.H.R. under the
729 leadership of Beth Bergeron. Ice cores dated by M.S., J.R.M.. ICP-MS and CFA measurements
730 performed by O.J.M, J.R.M., N.J.C., L.L, D.P., M.S.. MSA measurements designed and performed by
731 M.G., E.S.

732

733 **Acknowledgements**

734 This research was funded by the National Science Foundation; grant numbers 1023672 and 1204176.

735

736 **References**

- 737 Abbatt, J., Oldridge, N., Symington, A., Chukalovskiy, V., McWhinney, R. D., Sjostedt, S. and Cox, R.
738 A.: Release of gas-phase halogens by photolytic generation of OH in frozen halide-nitrate solutions: an
739 active halogen formation mechanism?, *J. Phys. Chem. A*, 114(23), 6527–33, doi:10.1021/jp102072t,
740 2010.
- 741 Abbatt, J. P. D.: Interactions of HBr, HCl, and HOBr With Supercooled Sulfuric- Acid-Solutions of
742 Stratospheric Composition, *J. Geophys. Res.*, 100(D7), 14009–14017, 1995.
- 743 Abbatt, J. P. D., Thomas, J. L., Abrahamsson, K., Boxe, C., Granfors, A., Jones, A. E., King, M. D.,
744 Saiz-Lopez, A., Shepson, P. B., Sodeau, J., Toohey, D. W., Toubin, C., von Glasow, R., Wren, S. N.
745 and Yang, X.: Halogen activation via interactions with environmental ice and snow in the polar lower
746 troposphere and other regions, *Atmos. Chem. Phys.*, 12(14), 6237–6271, doi:10.5194/acp-12-6237-
747 2012, 2012.
- 748 Abram, N. J., Wolff, E. W. and Curran, M. A. J.: A review of sea ice proxy information from polar ice
749 cores, *Quat. Sci. Rev.*, 79, 168–183, doi:10.1016/j.quascirev.2013.01.011, 2013.
- 750 Appenzeller, C., Schwander, J., Sommer, S. and Stocker, T. F.: The North Atlantic Oscillation and its
751 imprint on precipitation and ice accumulation in Greenland, *Geophys. Res. Lett.*, 25(11), 1939,
752 doi:10.1029/98GL01227, 1998.
- 753 Arienzo, M. M., McConnell, J. R., Chellman, N., Criscitiello, A. S., Curran, M., Fritzsche, D., Kipfstuhl,
754 S., Mulvaney, R., Nolan, M., Opel, T., Sigl, M. and Steffensen, J. P.: A Method for Continuous ²³⁹Pu
755 Determinations in Arctic and Antarctic Ice Cores, *Environ. Sci. Technol.*, 50(13), 7066–7073,
756 doi:10.1021/acs.est.6b01108, 2016.
- 757 Barrie, L. A., Hoff, R. M. and Daggupaty, S. M.: The influence of mid-litudinal pollution sources on
758 haze in the Canadian arctic, *Atmos. Environ.*, 15(8), 1407–1419, doi:10.1016/0004-6981(81)90347-4,
759 1981.
- 760 Berg, W. W., Sperry, P. D., Rahn, K. A. and Gladney, E. S.: Atmospheric Bromine in the Arctic, *J.*
761 *Geophys. Res.*, 88, 6719–6736, doi:10.1029/JC088iC11p06719, 1983.
- 762 Bertram, F. J. and Kolowich, J. B.: A study of methyl bromide emissions from automobiles burning
763 leaded gasoline using standardized vehicle testing procedures, *Geophys. Res. Lett.*, 27(9), 1423–1426,
764 doi:10.1029/1999GL011008, 2000.
- 765 Bowen, H. J. M.: Environmental chemistry of the elements / H. J. M. Bowen, BOOK, Academic Press,

766 London ; New York., 1979.

767 Chellman, N. J., Hastings, M. G. and McConnell, J. R.: Increased nitrate and decreased $\delta^{15}\text{N-NO}_3^-$ in
768 the Greenland Arctic after 1940 attributed to North American oil burning, *Cryosph. Discuss.*, 1–22,
769 doi:10.5194/tc-2016-163, 2016.

770 Chen, Q. S., Bromwich, D. H. and Bai, L.: Precipitation over Greenland retrieved by a dynamic method
771 and its relation to cyclonic activity, *J. Clim.*, 10(5), 839–870, 1997.

772 Chu, L. and Anastasio, C.: Formation of hydroxyl radical from the photolysis of frozen hydrogen
773 peroxide, *J. Phys. Chem. A*, 109(28), 6264–6271, doi:10.1021/jp051415f, 2005.

774 Curran, M. A. J. and Jones, G. B.: Dimethyl sulfide in the Southern Ocean: Seasonality and flux, *J.*
775 *Geophys. Res.*, 105(D16), 20451, doi:10.1029/2000JD900176, 2000.

776 Curran, M. A. J., van Ommen, T. D., Morgan, V. I., Phillips, K. L. and Palmer, A. S.: Ice core evidence
777 for Antarctic sea ice decline since the 1950s., *Science*, 302(5648), 1203–1206,
778 doi:10.1126/science.1087888, 2003.

779 Draxler, R. R. and Hess, G. D.: An Overview of the HYSPLIT_4 Modelling System for Trajectories,
780 Dispersion, and Deposition., *Aust. Meteorol. Mag.*, 47(June 1997), 295–308, 1998.

781 Fan, S.-M. and Jacob, D. J.: Surface ozone depletion in Arctic spring sustained by bromine reactions on
782 aerosols, *Nature*, 359(6395), 522–524, doi:10.1038/359522a0, 1992.

783 Felix, J. D. and Elliott, E. M.: The agricultural history of human-nitrogen interactions as recorded in ice
784 core $\delta^{15}\text{N-NO}_3^-$, *Geophys. Res. Lett.*, 40(8), 1642–1646, doi:10.1002/grl.50209, 2013.

785 Finlayson-Pitts, B. J.: The Tropospheric Chemistry of Sea Salt: A Molecular-Level View of the
786 Chemistry of NaCl and NaBr, *Chem. Rev.*, 103(12), 4801–4822, doi:10.1021/cr020653t, 2003.

787 Fischer, H. and Wagenbach, D.: Large-scale spatial trends in recent firn chemistry along an east-west
788 transect through central Greenland, *Atmos. Environ.*, 30(19), 3227–3238, doi:10.1016/1352-
789 2310(96)00092-1, 1996.

790 Frinak, E. K. and Abbatt, J. P. D.: Br₂ production from the heterogeneous reaction of gas-phase OH
791 with aqueous salt solutions: Impacts of acidity, halide concentration, and organic surfactants., *J. Phys.*
792 *Chem. A*, 110(35), 10456–64, doi:10.1021/jp063165o, 2006.

793 George, I. J. and Anastasio, C.: Release of gaseous bromine from the photolysis of nitrate and hydrogen
794 peroxide in simulated sea-salt solutions, *Atmos. Environ.*, 41(3), 543–553,
795 doi:10.1016/j.atmosenv.2006.08.022, 2007.

796 Hunke, E. C., Notz, D., Turner, A. K. and Vancoppenolle, M.: The multiphase physics of sea ice: a
797 review for model developers, *Cryosph.*, 5(4), 989–1009, doi:10.5194/tc-5-989-2011, 2011.

798 Jacobi, H. W., Kleffmann, J., Villena, G., Wiesen, P., King, M., France, J., Anastasio, C. and Staebler,
799 R.: Role of nitrite in the photochemical formation of radicals in the snow, *Environ. Sci. Technol.*, 48(1),
300 165–172, doi:10.1021/es404002c, 2014.

301 Jaffrezo, J. L., Davidson, C. I., Legrand, M. and Dibb, J. E.: Sulfate and MSA in the air and snow on
302 the Greenland Ice Sheet, *J. Geophys. Res.*, 99(D1), 1241–1253, doi:10.1029/93JD02913, 1994.

303 Kahl, J. D. W., Martinez, D. A., Kuhns, H., Davidson, C. I., Jafferezo, J. L. and Harris, J. M.: Air mass
304 trajectories to Summit, Greenland : A 44-year climatology and some episodic events, *J. Geophys. Res.*
305 *Ocean.*, 102(C12), 26861–26875, 1997.

306 Kerkweg, A., Jöckel, P., Warwick, N., Gebhardt, S., Brenninkmeijer, C. A. M. and Lelieveld, J.:
307 Consistent simulation of bromine chemistry from the marine boundary layer to the stratosphere – Part
308 2 : Bromocarbons, *Atmos. Chem. Phys. Discuss.*, 8(3), 9477–9530, doi:10.5194/acpd-8-9477-2008,
309 2008.

310 Kinnard, C., Zdanowicz, C. M., Koerner, R. M. and Fisher, D. A.: A changing Arctic seasonal ice zone:
311 Observations from 1870-2003 and possible oceanographic consequences, *Geophys. Res. Lett.*, 35(2),
312 2–6, doi:10.1029/2007GL032507, 2008.

313 Lamarque, J.-F., Dentener, F., McConnell, J., Ro, C.-U., Shaw, M., Vet, R., Bergmann, D., Cameron-
314 Smith, P., Dalsoren, S., Doherty, R., Faluvegi, G., Ghan, S. J., Josse, B., Lee, Y. H., MacKenzie, I. A.,
315 Plummer, D., Shindell, D. T., Skeie, R. B., Stevenson, D. S., Strode, S., Zeng, G., Curran, M., Dahl-
316 Jensen, D., Das, S., Fritzsche, D. and Nolan, M.: Multi-model mean nitrogen and sulfur deposition from
317 the Atmospheric Chemistry and Climate Model Intercomparison Project (ACCMIP): evaluation of
318 historical and projected future changes, *Atmos. Chem. Phys.*, 13(16), 7997–8018, doi:10.5194/acp-13-
319 7997-2013, 2013.

320 Langendörfer, U., Lehrer, E., Wagenbach, D. and Platt, U.: Observation of filterable bromine
321 variabilities during Arctic tropospheric ozone depletion events in high (1 hour) time resolution, *J.*
322 *Atmos. Chem.*, 34(1), 39–54, doi:10.1023/A:1006217001008, 1999.

323 Legrand, M., Hammer, C., De Angelis, M., Savarino, J., Delmas, R., Clausen, H. and Johnsen, S. J.:
324 Sulfur-containing species (methanesulfonate and SO₄) over the last climatic cycle in the Greenland Ice
325 Core Project (central Greenland) ice core, *J. Geophys. Res.*, 102(C12), 26663, doi:10.1029/97JC01436,
326 1997.

327 Lehrer, E., Wagenbach, D. and Platt, U.: Aerosol chemical composition during tropospheric ozone
328 depletion at Ny Ålesund/Svalbard, *Tellus B*, 49(5), doi:10.3402/tellusb.v49i5.15987, 1997.

329 Leu, E., Mundy, C. J., Assmy, P., Campbell, K., Gabrielsen, T. M., Gosselin, M., Juul-Pedersen, T. and
330 Gradinger, R.: Arctic spring awakening - Steering principles behind the phenology of vernal ice algal
331 blooms, *Prog. Oceanogr.*, 139, 151–170, doi:10.1016/j.pocean.2015.07.012, 2015.

332 Li, S.-M. and Barrie, L. A.: Biogenic sulfur aerosol in the Arctic troposphere: 1. Contributions to total
333 sulfate, *J. Geophys. Res.*, 98(D11), 20613, doi:10.1029/93JD02234, 1993.

334 Macias Fauria, M., Grinsted, A., Helama, S., Moore, J., Timonen, M., Martma, T., Isaksson, E. and
335 Eronen, M.: Unprecedented low twentieth century winter sea ice extent in the Western Nordic Seas
336 since A.D. 1200, *Clim. Dyn.*, 34(6), 781–795, doi:10.1007/s00382-009-0610-z, 2010.

337 Mann, M. E., Bradley, R. S. and Hughes, M. K.: Global-scale temperature patterns and climate forcing
338 over the past six centuries, *Nature*, 392(6678), 779–787, doi:10.1038/33859, 1998.

339 Maselli, O. J., Fritzsche, D., Layman, L., McConnell, J. R. and Meyer, H.: Comparison of water isotope-
340 ratio determinations using two cavity ring-down instruments and classical mass spectrometry in
341 continuous ice-core analysis., *Isotopes Environ. Health Stud.*, 49(September 2014), 387–98,
342 doi:10.1080/10256016.2013.781598, 2013.

343 McConnell, J. R. and Edwards, R.: Coal burning leaves toxic heavy metal legacy in the Arctic., *Proc.*
344 *Natl. Acad. Sci. U. S. A.*, 105(34), 12140–12144, doi:10.1073/pnas.0803564105, 2008.

345 McConnell, J. R., Lamorey, G. W., Lambert, S. W. and Taylor, K. C.: Continuous ice-core chemical
346 analyses using inductively coupled plasma mass spectrometry., *Environ. Sci. Technol.*, 36(775), 7–11,
347 doi:10.1021/es011088z, 2002.

348 McConnell, J. R., Edwards, R., Kok, G. L., Flanner, M. G., Zender, C. S., Saltzman, E. S., Banta, J. R.,
349 Pasteris, D. R., Carter, M. M. and Kahl, J. D. W.: 20th-Century Industrial Black Carbon Emissions
350 Altered Arctic Climate Forcing, *Science*, 317, 1381–1384, doi:10.1126/science.1144856, 2007.

351 Millero, F. J.: The Physical Chemistry of Seawater, *Annu. Rev. Earth Planet. Sci.*, 2(1), 101–150,
352 doi:10.1146/annurev.ea.02.050174.000533, 1974.

353 Moldanová, J. and Ljungström, E.: Sea-salt aerosol chemistry in coastal areas: A model study, *J.*
354 *Geophys. Res.*, 106, 1271, doi:10.1029/2000JD900462, 2001.

355 Montzka, S. and Reimann, S.: Scientific Assessment of Ozone Depletion 2010: Scientific Summary
356 Chapter 1 Ozone-Depleting Substances (ODSs) and Related Chemicals. [online] Available from:

357 <http://www.esrl.noaa.gov/csd/assessments/ozone/2010/summary/ch1.html> (Accessed 23 December
358 2015), 2010.

359 Morin, S., Savarino, J., Frey, M. M., Yan, N., Bekki, S., Bottenheim, J. and Martins, J. M. F.: Tracing
360 the origin and fate of NO_x in the Arctic atmosphere using stable isotopes in nitrate., *Science*, 322(5902),
361 730–2, doi:10.1126/science.1161910, 2008.

362 Mulvaney, R., Pasteur, E. C., Peel, D. A., Saltzman, E. S. and Whung, P.-Y.: The ratio of MSA to non-
363 sea-salt sulphate in Antarctic Peninsula ice cores, *Tellus B*, 44(4), doi:10.3402/tellusb.v44i4.15457,
364 1992.

365 Nghiem, S. V., Rigor, I. G., Richter, A., Burrows, J. P., Shepson, P. B., Bottenheim, J., Barber, D. G.,
366 Steffen, A., Latonas, J., Wang, F., Stern, G., Clemente-Colón, P., Martin, S., Hall, D. K., Kaleschke, L.,
367 Tackett, P., Neumann, G. and Asplin, M. G.: Field and satellite observations of the formation and
368 distribution of Arctic atmospheric bromine above a rejuvenated sea ice cover, *J. Geophys. Res. Atmos.*,
369 117(D17), n/a-n/a, doi:10.1029/2011JD016268, 2012.

370 Nriagu, J. O.: The rise and fall of leaded gasoline, *Sci. Total Environ.*, 92, 13–28, 1990.

371 NSIDC, National Snow and Ice Data Center, [online] Available from:
372 <http://nsidc.org/cryosphere/seaice/data/terminology.html> (Accessed December 2013).

373 O'Dwyer, J., Isaksson, E., Vinje, T., Jauhiainen, T., Moore, J., Pohjola, V., Vaikmae, R. and van de
374 Wal, R. S. W.: Methanesulfonic acid in a Svalbard ice core as an indicator of ocean climate, *Geophys.*
375 *Res. Lett.*, 27(8), 1159–1162, doi:10.1029/1999GL011106, 2000.

376 Ordóñez, C., Lamarque, J.-F., Tilmes, S., Kinnison, D. E., Atlas, E. L., Blake, D. R., Sousa Santos, G.,
377 Brasseur, G. and Saiz-Lopez, A.: Bromine and iodine chemistry in a global chemistry-climate model:
378 description and evaluation of very short-lived oceanic sources, *Atmos. Chem. Phys.*, 12(3), 1423–1447,
379 doi:10.5194/acp-12-1423-2012, 2012.

380 Oudijk, G.: The Rise and Fall of Organometallic Additives in Automotive Gasoline, *Environ. Forensics*,
381 11(933126918), 17–49, doi:10.1080/15275920903346794, 2010.

382 Parrella, J. P., Jacob, D. J., Liang, Q., Zhang, Y., Mickley, L. J., Miller, B., Evans, M. J., Yang, X., Pyle,
383 J. A., Theys, N. and Van Roozendael, M.: Tropospheric bromine chemistry: implications for present
384 and pre-industrial ozone and mercury, *Atmos. Chem. Phys.*, 12(15), 6723–6740, doi:10.5194/acp-12-
385 6723-2012, 2012.

386 Pasteris, D. R., McConnell, J. R. and Edwards, R.: High-resolution, continuous method for measurement

387 of acidity in ice cores, *Environ. Sci. Technol.*, 46, 1659–1666, doi:10.1021/es202668n, 2012.

388 Pratt, K. A., Custard, K. D., Shepson, P. B., Douglas, T. A., Pöhler, D., General, S., Zielcke, J., Simpson,
389 W. R., Platt, U., Tanner, D. J., Gregory Huey, L., Carlsen, M. and Stirm, B. H.: Photochemical
390 production of molecular bromine in Arctic surface snowpacks, *Nat. Geosci.*, 6(5), 351–356,
391 doi:10.1038/ngeo1779, 2013.

392 Rankin, A. M., Wolff, E. W. and Martin, S.: Frost flowers: Implications for tropospheric chemistry and
393 ice core interpretation, *J. Geophys. Res. Atmos.*, 107(D23), 4683, doi:10.1029/2002JD002492, 2002.

394 Rayner, N. A.: Global analyses of sea surface temperature, sea ice, and night marine air temperature
395 since the late nineteenth century, *J. Geophys. Res.*, 108(D14), 4407, doi:10.1029/2002JD002670, 2003.

396 Röthlisberger, R., Bigler, M., Hutterli, M., Sommer, S., Stauffer, B., Junghans, H. G. and Wagenbach,
397 D.: Technique for continuous high-resolution analysis of trace substances in firn and ice cores, *Environ.*
398 *Sci. Technol.*, 34(2), 338–342, doi:10.1021/es9907055, 2000.

399 Röthlisberger, R., Mulvaney, R., Wolff, E. W., Hutterli, M. a., Bigler, M., Sommer, S. and Jouzel, J.:
900 Dust and sea salt variability in central East Antarctica (Dome C) over the last 45 kyrs and its implications
901 for southern high-latitude climate, *Geophys. Res. Lett.*, 29(20), 1–4, doi:10.1029/2003GL016936, 2002.

902 Saltzman, E. S., Dioumaeva, I. and Finley, B. D.: Glacial/interglacial variations in methanesulfonate
903 (MSA) in the Siple Dome ice core, West Antarctica, *Geophys. Res. Lett.*, 33(11), 1–4,
904 doi:10.1029/2005GL025629, 2006.

905 Sander, R., Rudich, Y., von Glasow, R. and Crutzen, P. J.: The role of BrNO₃ in marine tropospheric
906 chemistry: A model study, *Geophys. Res. Lett.*, 26(18), 2857–2860, doi:10.1029/1999GL900478, 1999.

907 Sander, R., Keene, W. C., Pszenny, A. A. P., Arimoto, R., Ayers, G. P., Baboukas, E., Cainey, J. M.,
908 Crutzen, P. J., Duce, R. A., Hönninger, G., Huebert, B. J., Maenhaut, W., Mihalopoulos, N., Turekian,
909 V. C. and Van Dingenen, R.: Inorganic bromine in the marine boundary layer: a critical review, *Atmos.*
910 *Chem. Phys.*, 3, 1301–1336, doi:10.5194/acp-3-1301-2003, 2003.

911 Schönhardt, A., Begoin, M., Richter, A., Wittrock, F., Kaleschke, L., Gómez Martín, J. C. and Burrows,
912 J. P.: Simultaneous satellite observations of IO and BrO over Antarctica, *Atmos. Chem. Phys.*, 12(14),
913 6565–6580, doi:10.5194/acp-12-6565-2012, 2012.

914 Sharma, S., Chan, E., Ishizawa, M., Toom-Sauntry, D., Gong, S. L., Li, S. M., Tarasick, D. W., Leaitch,
915 W. R., Norman, A., Quinn, P. K., Bates, T. S., Levasseur, M., Barrie, L. A. and Maenhaut, W.: Influence
916 of transport and ocean ice extent on biogenic aerosol sulfur in the Arctic atmosphere, *J. Geophys. Res.*

017 Atmos., 117(12), n/a-n/a, doi:10.1029/2011JD017074, 2012.

018 Sigl, M., McConnell, J. R., Layman, L., Maselli, O. J., McGwire, K., Pasteris, D., Dahl-Jensen, D.,
019 Steffensen, J. P., Vinther, B., Edwards, R., Mulvaney, R. and Kipfstuhl, S.: A new bipolar ice core
020 record of volcanism from WAIS Divide and NEEM and implications for climate forcing of the last 2000
021 years, *J. Geophys. Res. Atmos.*, 118(3), 1151–1169, doi:10.1029/2012JD018603, 2013.

022 Sigl, M., Winstrup, M., McConnell, J. R., Welten, K. C., Plunkett, G., Ludlow, F., Büntgen, U., Caffee,
023 M., Chellman, N., Dahl-Jensen, D., Fischer, H., Kipfstuhl, S., Kostick, C., Maselli, O. J., Mekhaldi, F.,
024 Mulvaney, R., Muscheler, R., Pasteris, D. R., Pilcher, J. R., Salzer, M., Schüpbach, S., Steffensen, J. P.,
025 Vinther, B. M. and Woodruff, T. E.: Timing and climate forcing of volcanic eruptions for the past 2,500
026 years, *Nature*, 523(7562), 543–9, doi:10.1038/nature14565, 2015.

027 Simpson, W. R., von Glasow, R., Riedel, K., Anderson, P., Ariya, P., Bottenheim, J., Burrows, J.,
028 Carpenter, L. J., Friess, U., Goodsite, M. E., Heard, D., Hutterli, M., Jacobi, H.-W., Kaleschke, L., Neff,
029 B., Plane, J., Platt, U., Richter, A., Roscoe, H., Sander, R., Shepson, P., Sodeau, J., Steffen, A., Wagner,
030 T. and Wolff, E.: Halogens and their role in polar boundary-layer ozone depletion, , 4375–4418,
031 doi:10.5194/acpd-7-4285-2007, 2007.

032 Sjostedt, S. J., Huey, L. G., Tanner, D. J., Peischl, J., Chen, G., Dibb, J. E., Lefer, B., Hutterli, M. A.,
033 Beyersdorf, A. J., Blake, N. J., Blake, D. R., Sueper, D., Ryerson, T., Burkhardt, J. and Stohl, A.:
034 Observations of hydroxyl and the sum of peroxy radicals at Summit, Greenland during summer 2003,
035 *Atmos. Environ.*, 41(24), 5122–5137, doi:10.1016/j.atmosenv.2006.06.065, 2007.

036 Smith, S. J., van Aardenne, J., Klimont, Z., Andres, R. J., Volke, A. and Delgado Arias, S.:
037 Anthropogenic sulfur dioxide emissions: 1850–2005, *Atmos. Chem. Phys.*, 11(3), 1101–1116,
038 doi:10.5194/acp-11-1101-2011, 2011.

039 Spolaor, A., Vallelonga, P., Plane, J. M. C., Kehrwald, N., Gabrieli, J., Varin, C., Turetta, C., Cozzi, G.,
040 Kumar, R., Boutron, C. and Barbante, C.: Halogen species record Antarctic sea ice extent over glacial-
041 interglacial periods, *Atmos. Chem. Phys.*, 13, 6623–6635, doi:10.5194/acp-13-6623-2013, 2013a.

042 Spolaor, A., Gabrieli, J., Martma, T., Kohler, J., Björkman, M. B., Isaksson, E., Varin, C., Vallelonga,
043 P., Plane, J. M. C. and Barbante, C.: Sea ice dynamics influence halogen deposition to Svalbard,
044 *Cryosph.*, 7(5), 1645–1658, doi:10.5194/tc-7-1645-2013, 2013b.

045 Spolaor, A., Vallelonga, P., Gabrieli, J., Martma, T., Björkman, M. P., Isaksson, E., Cozzi, G., Turetta,
046 C., Kjær, H. A., Curran, M. A. J., Moy, A. D., Schönhardt, A., Blechschmidt, A.-M., Burrows, J. P.,
047 Plane, J. M. C. and Barbante, C.: Seasonality of halogen deposition in polar snow and ice, *Atmos. Chem.*

948 Phys., 14(18), 9613–9622, doi:10.5194/acp-14-9613-2014, 2014.

949 Spolaor, A., Opel, T., McConnell, J. R., Maselli, O. J., Spreen, G., Varin, C., Kirchgeorg, T., Fritzsche,
950 D., Saiz-Lopez, A. and Vallelonga, P.: Halogen-based reconstruction of Russian Arctic sea ice area
951 from the Akademii Nauk ice core (Severnaya Zemlya), *Cryosph.*, 10, 245–256, doi:10.5194/tcd-9-4407-
952 2015, 2016.

953 Sturges, W. T. and Harrison, R. M.: Bromine:Lead ratios in airborne particles from urban and rural sites,
954 *Atmos. Environ.*, 20(3), 577–588, doi:10.1016/0004-6981(86)90101-0, 1986.

955 Thomas, J. L., Dibb, J. E., Huey, L. G., Liao, J., Tanner, D., Lefer, B., von Glasow, R. and Stutz, J.:
956 Modeling chemistry in and above snow at Summit, Greenland – Part 2: Impact of snowpack chemistry
957 on the oxidation capacity of the boundary layer, *Atmos. Chem. Phys.*, 12(14), 6537–6554,
958 doi:10.5194/acp-12-6537-2012, 2012.

959 Thomas, V. M., Bedford, J. A. and Cicerone, R. J.: Bromine emissions from leaded gasoline, *Geophys.*
960 *Res. Lett.*, 24(11), 1371–1374, doi:10.1029/97GL01243, 1997.

961 Vestreng, V., Ntziachristos, L., Semb, A., Reis, S., Isaksen, I. S. A. and Tarrasón, L.: Evolution of NO_x
962 emissions in Europe with focus on road transport control measures, *Atmos. Chem. Phys.*, 9(4), 1503–
963 1520, doi:10.5194/acp-9-1503-2009, 2009.

964 Wagner, T., Leue, C., Wenig, M., Pfeilsticker, K. and Platt, U.: Spatial and temporal distribution of
965 enhanced boundary layer BrO concentrations measured by the GOME instrument aboard ERS-2, *J.*
966 *Geophys. Res.*, 106(D20), 24225, doi:10.1029/2000JD000201, 2001.

967 Wais Divide Project Memembers: Onset of deglacial warming in West Antarctica driven by local orbital
968 forcing., *Nature*, 500(7463), 440–4, doi:10.1038/nature12376, 2013.

969 Walsh, J. E.: A data set on Northern Hemisphere sea ice extent, *Natl. Snow Ice Data Cent.*, 49–51, 1978.

970 Weißbach, S., Wegner, A., Opel, T., Oerter, H., Vinther, B. M. and Kipfstuhl, S.: Spatial and temporal
971 oxygen isotope variability in northern Greenland - implications for a new climate record over the past
972 millennium, *Clim. Past Discuss.*, 11(3), 2341–2388, doi:10.5194/cpd-11-2341-2015, 2015.

973 Weller, R.: Postdepositional losses of methane sulfonate, nitrate, and chloride at the European Project
974 for Ice Coring in Antarctica deep-drilling site in Dronning Maud Land, Antarctica, *J. Geophys. Res.*,
975 109(D7), 1–9, doi:10.1029/2003JD004189, 2004.

976 WMO: Scientific Assessment of Ozone Depletion: 1994. Chapter 10: Methyl Bromide, Geneva., 1995.

977 WMO: Scientific Assessment of Ozone Depletion: 2002. Chapter 1: Controlled Substances and Other

078 Source Gases., 2002.

079 Wolff, E. W.: Ice sheets and nitrogen, *Philos. Trans. R. Soc. Lond. B. Biol. Sci.*, 368,
080 doi:10.1098/rstb.2013.0127, 2013.

081 Wolff, E. W., Rankin, A. M. and Röthlisberger, R.: An ice core indicator of Antarctic sea ice
082 production?, *Geophys. Res. Lett.*, 30(22), 2–5, doi:10.1029/2003GL018454, 2003.

083 Xu, L., Russell, L. M., Somerville, R. C. J. and Quinn, P. K.: Frost flower aerosol effects on Arctic
084 wintertime longwave cloud radiative forcing, *J. Geophys. Res. Atmos.*, 118(23), 13282–13291,
085 doi:10.1002/2013JD020554, 2013.

086 Yang, X., Pyle, J. A. and Cox, R. A.: Sea salt aerosol production and bromine release: Role of snow on
087 sea ice, *Geophys. Res. Lett.*, 35(16), 1–5, doi:10.1029/2008GL034536, 2008.

088 Yang, X., Pyle, J. A., Cox, R. A., Theys, N. and Van Roozendaal, M.: Snow-sourced bromine and its
089 implications for polar tropospheric ozone, *Atmos. Chem. Phys.*, 10(16), 7763–7773, doi:10.5194/acp-
090 10-7763-2010, 2010.

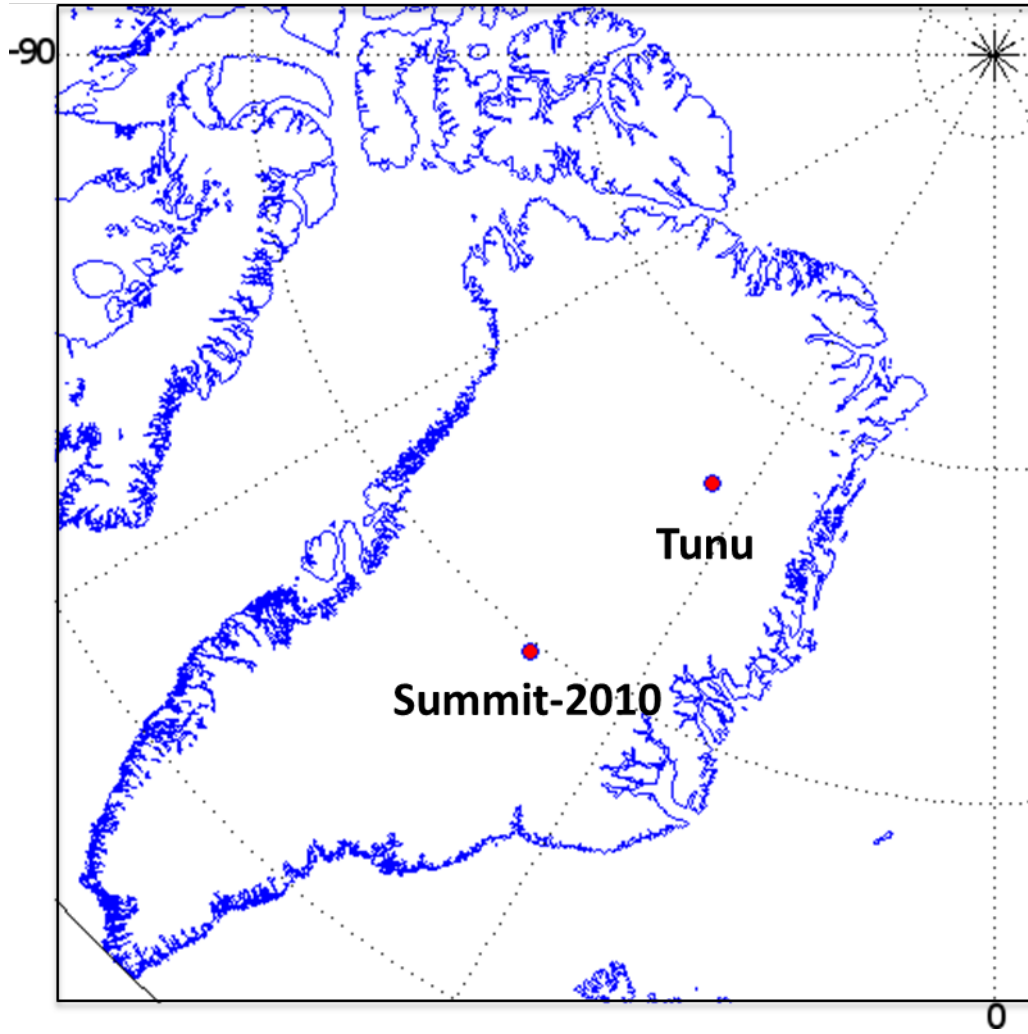
091 Yung, Y. L., Pinto, J. P., Watson, R. T. and Sander, S. P.: Atmospheric Bromine and Ozone
092 Perturbations in the Lower Stratosphere, *J. Atmos. Sci.*, 37(2), 339–353, doi:10.1175/1520-
093 0469(1980)037<0339:ABAOPI>2.0.CO;2, 1980.

094

095

996

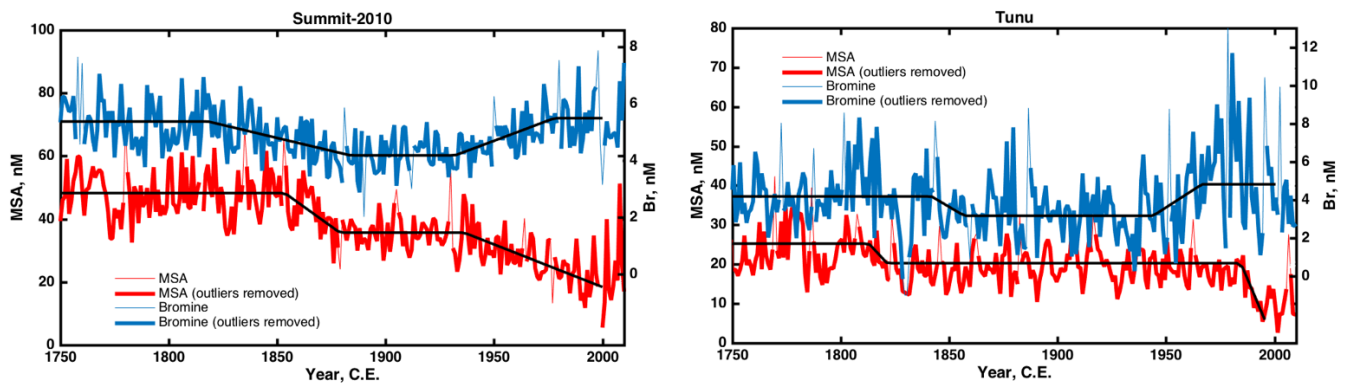
997



998

999 **Figure 1.** Locations of ice cores used in this study. Summit-2010: (72°20'N 38°17'24"W), Tunu: (78°
100 2' 5.5"N, 33° 52' 48"W)

101

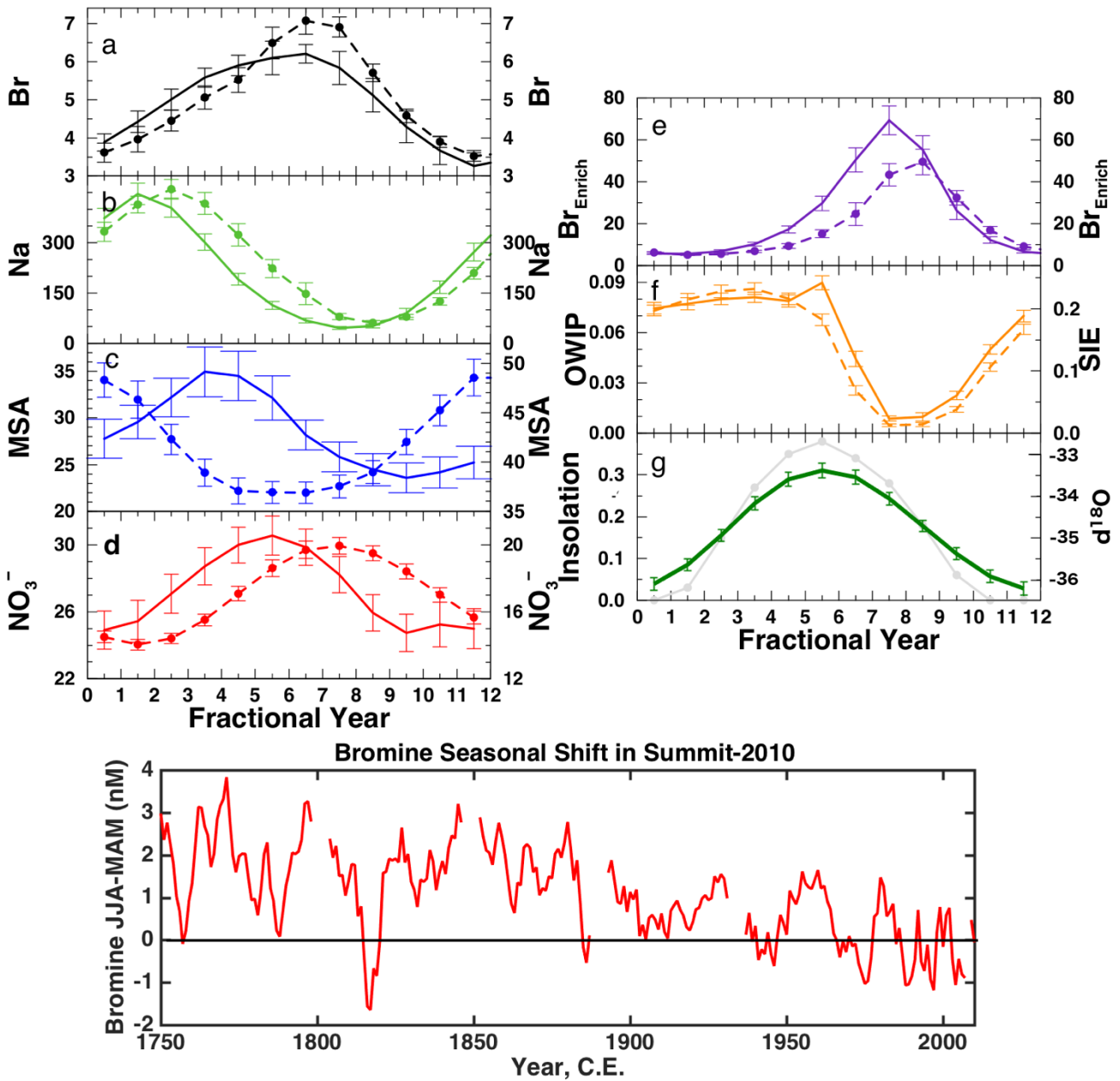


002

003

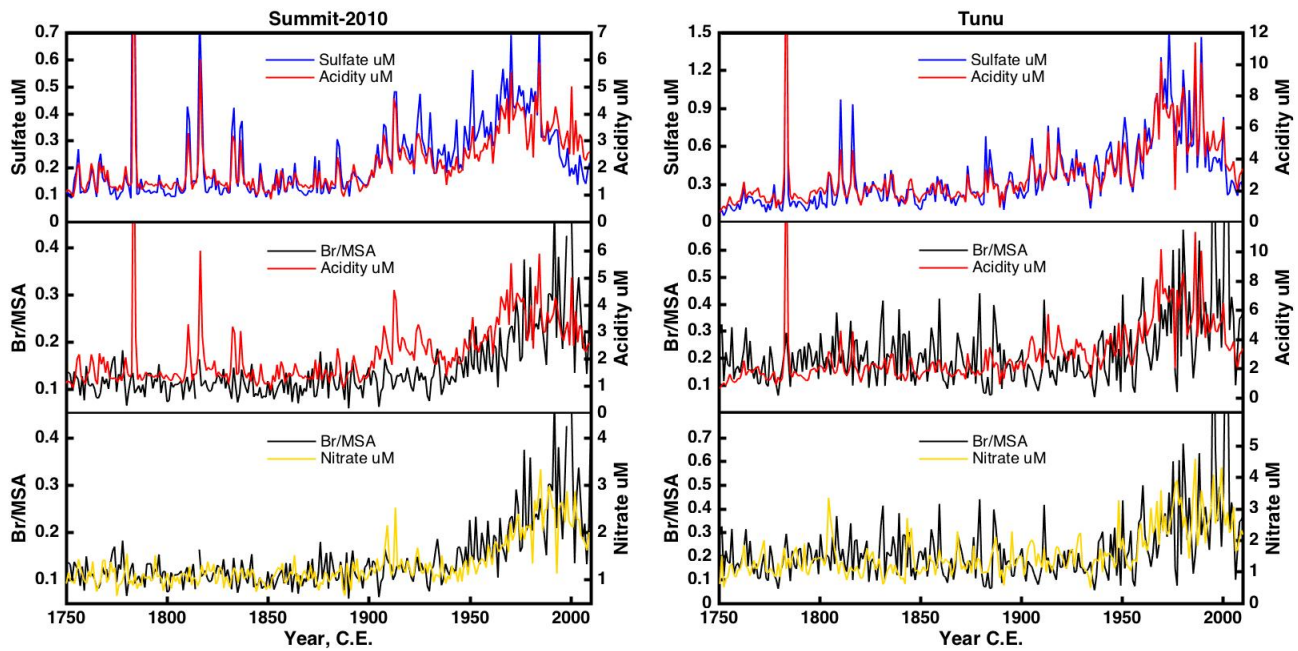
004 **Figure 2.** Annual record of bromine (thin blue) and MSA (thin red). Annual record of bromine (thick
 005 blue) and MSA (thick red) with outlying spikes removed using a 25 year running average filter described
 006 by Sigl et al. (2013). All records were fit with a 3 step linear regression (black) and the results of the
 007 fits which identify the timing of inflection points are summarized in Table S1. The time-series have
 008 been plotted to match the signal variability in the preindustrial era (1750-1850 C.E.).

009



012 **Figure 3.** Upper plots: Average seasonal cycle of species in the Summit-2010 ice core. The left-hand Y
 013 axes are associated with the solid lines, and the right-hand Y axes associated with the dashed lines.
 014 Dashed lines (a-e): Average seasonal cycle from depths 43.5 – 87.3 m (years 1742-1900). Solid lines
 015 (a-e): Average seasonal cycle from 0-43.5 m (years 1900-2010). Error bars indicate the standard error
 016 of the monthly value. (a) Total bromine, (b) total sodium, (c) MSA, (d) nitrate. Units for (a-d) are nM.
 017 Note that the seasonal cycle in bromine appears to broaden in the 1900-2010 period (see lower panel).
 018 Note also that the MSA maximum shifts from spring in the shallowest part of the ice core (solid line) to
 019 winter in the deepest part of the ice core (dashed line) due to post-depositional effects (see Fig. S1). (e)

020 Average seasonal cycle in bromine enrichment (relative to sea salt sodium, see Eq. (4)). (f-right) The
021 sea ice extent (SIE, $\times 10^6 \text{ km}^2$) within an area of the East Greenland coast [70° – 63° N, 15° – 45° W], (f
022 – left) Area of open water within the sea ice pack (OWIP, $\times 10^6 \text{ km}^2$) for the area defined by SIE. (g-
023 left) Solar insolation at 12 GMT at the latitude of Summit (eosweb.larc.nasa.gov). (g-right) Annual
024 cycle of the $\delta^{18}\text{O}$ water signal averaged over 1900-2010 C.E. Lower plot: Broadening of bromine
025 seasonal cycle in the Summit-2010 ice core. The difference between the summer and spring bromine
026 signal (JJA-MAM) was monitored over the length of the entire ice core. In the preindustrial era (pre-
027 1850) bromine peaks in summer; realised as positive values of JJA-MAM. After 1900 there is a marked
028 broadening of the seasonal signal towards spring and by ~ 1970 the seasonal signal maximum is routinely
029 shared between summer and spring realised as an averaged JJA-MAM of approximately zero.
030



331

332

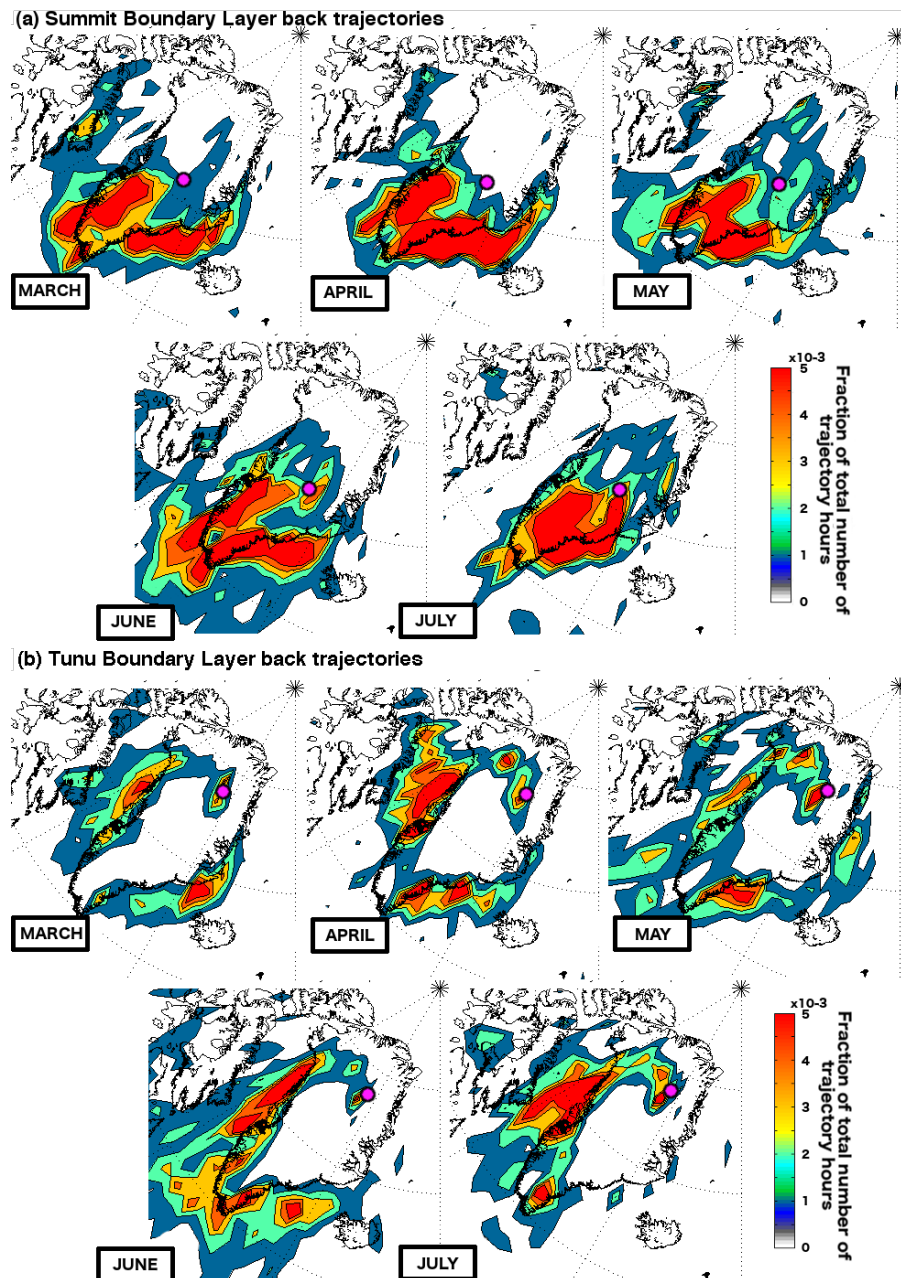
333 **Figure 4.** Comparison between the measured total sulfur (shown as sulfate) and acidity records from
 334 each ice core (top panels). The acidity record is dominated by the influence of the sulfur species until
 335 the early 21st century when the NO_x pollution remains elevated whilst anthropogenic sulfur sources are
 336 depleted resulting in a slight relative elevation of the total acidity relative to total sulfur concentrations.
 337 The large spikes in the acidity and sulfur records are identified as volcanic events. The ice core records
 338 cover the period of the 1783 Laki eruption as well as the Unknown 1909 eruption and Tambora eruption
 339 (Indonesia) in 1815 (Sigl et al., 2013). Comparison between Br/MSA and total acidity (center panels)
 340 and nitrate (NO_3^- , bottom panels) measured in the ice cores. The Br/MSA ratio follows the total acidity
 341 record closely except where the record is dominated by the sulfur component (e.g. early 1900s). Of the
 342 two major acidic species the Br/MSA follows the nitrate most closely at both ice core sites.

343

344

345

346



047

048 **Figure 5.** Air mass back trajectories from the (a) Summit-2010 and (b) Tunu ice core sites over the
 049 period 2005-2013 C.E. Maps display the fraction of the total number of trajectory hours (ranging
 050 between 21400-25500 hr month^{-1}) spent at altitudes under 500 m. Back trajectories were allowed to
 051 travel for 10 days. New trajectories were started every 12 hours. Map grid resolution is $2^\circ \times 2^\circ$. Ice core
 052 locations are shown by a pink circle. Maps show that air masses consistently arrive at Summit from the
 053 SE Greenland coast with a smaller contribution from the SW coast. Air masses consistently arrive at
 054 Tunu from the western Greenland coast with a smaller contribution from the SE and NE coast. The air
 055 mass originating from the NE coast is most dominant in May and comparison with the total vertical
 056 column profile (Fig. S8) shows it is confined to lower altitudes unlike those from the west coast.

357

358

Figure 6 consists of two main panels, (a) and (b), each with an upper map and lower time-series plots. Panel (a) is titled '1900-2010' and 'May SIC Vs Summit-2010 MSA'. The upper map shows a correlation coefficient (R) between May SIC and MSA, with a color scale from -1 (blue) to 1 (red). A black outline indicates a region of interest in the Arctic. The lower plot shows 'Summit-2010' data from 1900 to 2010, with 'May: $r = 0.58, p < 0.001$ '. It includes three y-axes: the left axis is 'May Open Water in the Ice Pack, $\text{km}^2 \times 10^5$ ' (0 to 2.5), the right axis is 'MSA' (0 to 50), and the right axis is 'enrich Br' (0 to 30). The legend includes 'OWIP' (black), 'MSA' (red), and 'MSA Outliers rem.' (orange). Panel (b) is titled '1979-2010' and 'March SIC Vs Summit-2010 MSA'. The upper map shows a correlation coefficient (R) between March SIC and MSA, with a color scale from -1 (blue) to 1 (red). The lower plot shows 'Summit-2010' data from 1980 to 2010, with 'March: $r = 0.4, p < 0.02$ '. It includes three y-axes: the left axis is 'March Open Water in the Ice Pack, $\text{km}^2 \times 10^5$ ' (6 to 14), the right axis is 'MSA' (0 to 50), and the right axis is 'enrich Br' (0 to 25). The legend includes 'OWIP' (black), 'MSA' (red), 'MSA Outliers rem.' (orange), 'Br Enrich' (green), and 'OWIP' (black). The bottom plot shows 'nsi Br' (black) and 'OWIP' (black) on the right axis (0 to 5).

359

360

361

362

363

364

365

366

367

368

369

370

371

372

373

374

375

376

Figure 6. Upper plot: Correlation map of monthly sea ice concentration (SIC) derived from the Summit-2010 ice core. The SIC map displayed corresponds to the month which shows the highest OWIP correlation (lower plot) with the annual MSA. Other monthly maps are shown in Fig. S9. (a) HadISST1 ICE dataset from 1900-2010 C.E. correlated with annual records of MSA (with outlier removed). Only locations that showed a SIC variability greater than 10% and have a significant correlation (t-test, $p < 0.05$) are displayed. The area of sea ice that is the likely source of MSA (as indicated by the air mass trajectories) are outlined in black [70° – 63° N, 0° – 45° W]. (b) As for (a) but focused on the satellite period 1979-2010 C.E. Lower plots: The correlation between the area of Open Water within the Ice Pack (OWIP) calculated within the black outlined areas shown on the upper maps and the annual MSA records (red, outliers removed – orange, nM). Summit-2010 MSA shows a significant, positive correlation with the amount of OWIP during spring within the integrated regions over both time periods. The highest correlations were found for March over the 1979-2010 period and May for the 1900-2010 period. In (b) if the MSA source region is enlarged to [70° – 63° N, 0° – 60° W] the March OWIP/MSA correlation increases slightly (from 0.38 to 0.4). The Summit-2010 enrBr(Na) (nM) and nsiBr (nM) records are also compared to the same OWIP records. Particularly over the longer time period there is little correlation between the series.

42

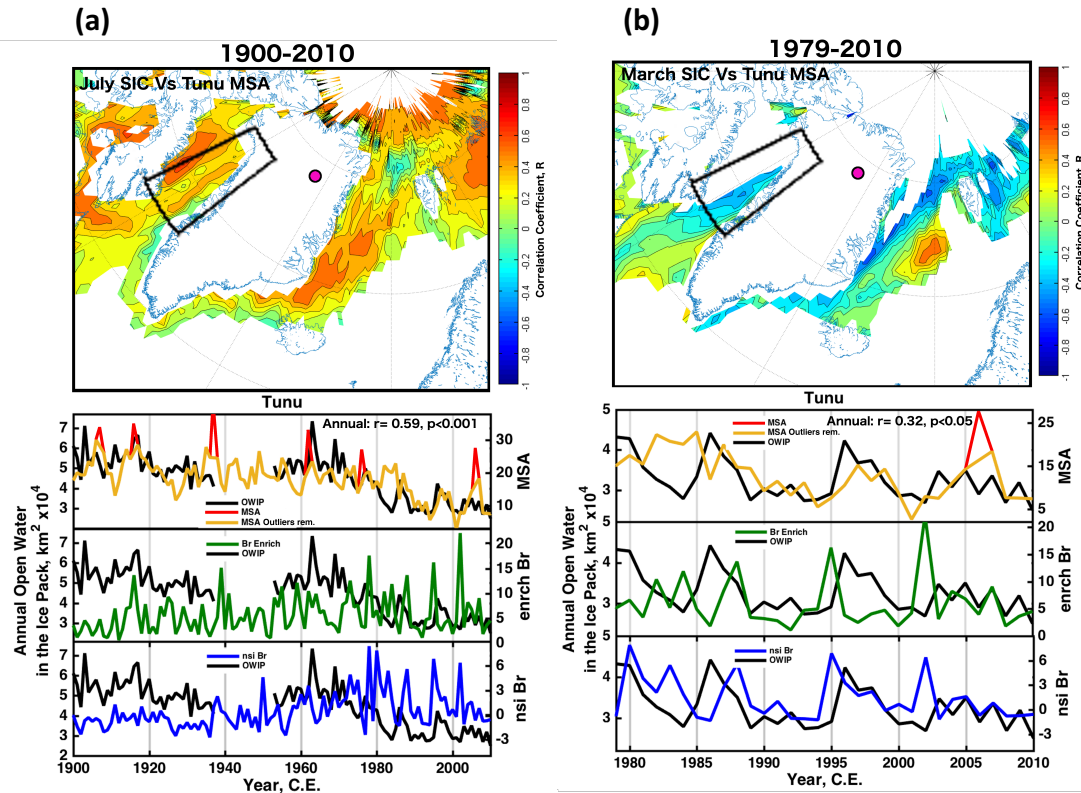
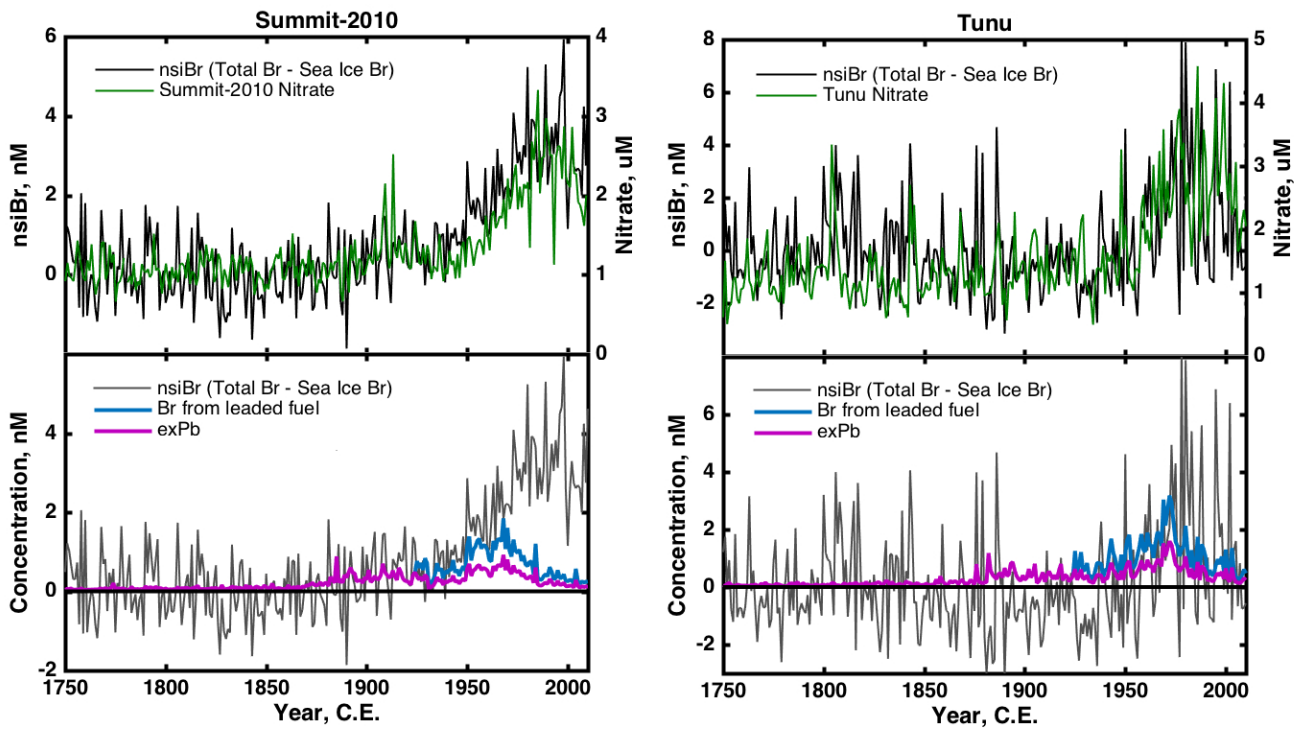


Figure 7. Upper plots: Correlation maps of monthly sea ice concentration (SIC) derived from the Tunu ice core. (a) HadISST1 ICE dataset from 1900-2012 C.E. correlated with annual records of MSA. The monthly SIC map displayed corresponds to the month which shows the highest OWIP correlation (lower plot) with the annual MSA. Other monthly maps are shown in Fig. S10. Only locations that showed a SIC variability greater than 10% and have a significant correlation (t-test, $p < 0.05$) are displayed. The area of sea ice that is the likely source of MSA (as indicated by the air mass trajectories) are outlined in black [77° – 67° N, 62° – 50° W]. (b) As for (a) but focused on the satellite period 1979-2012 C.E. Lower plots: The correlation between the area of Open Water within the Ice Pack (OWIP) calculated within the black outlined areas shown on the upper maps and the annual MSA records (red, outliers removed - orange). The Tunu enrBr(Na) (nM) and nsiBr (nM) records are also compared to the same OWIP records and show poor correlation, particularly over the longer time period.



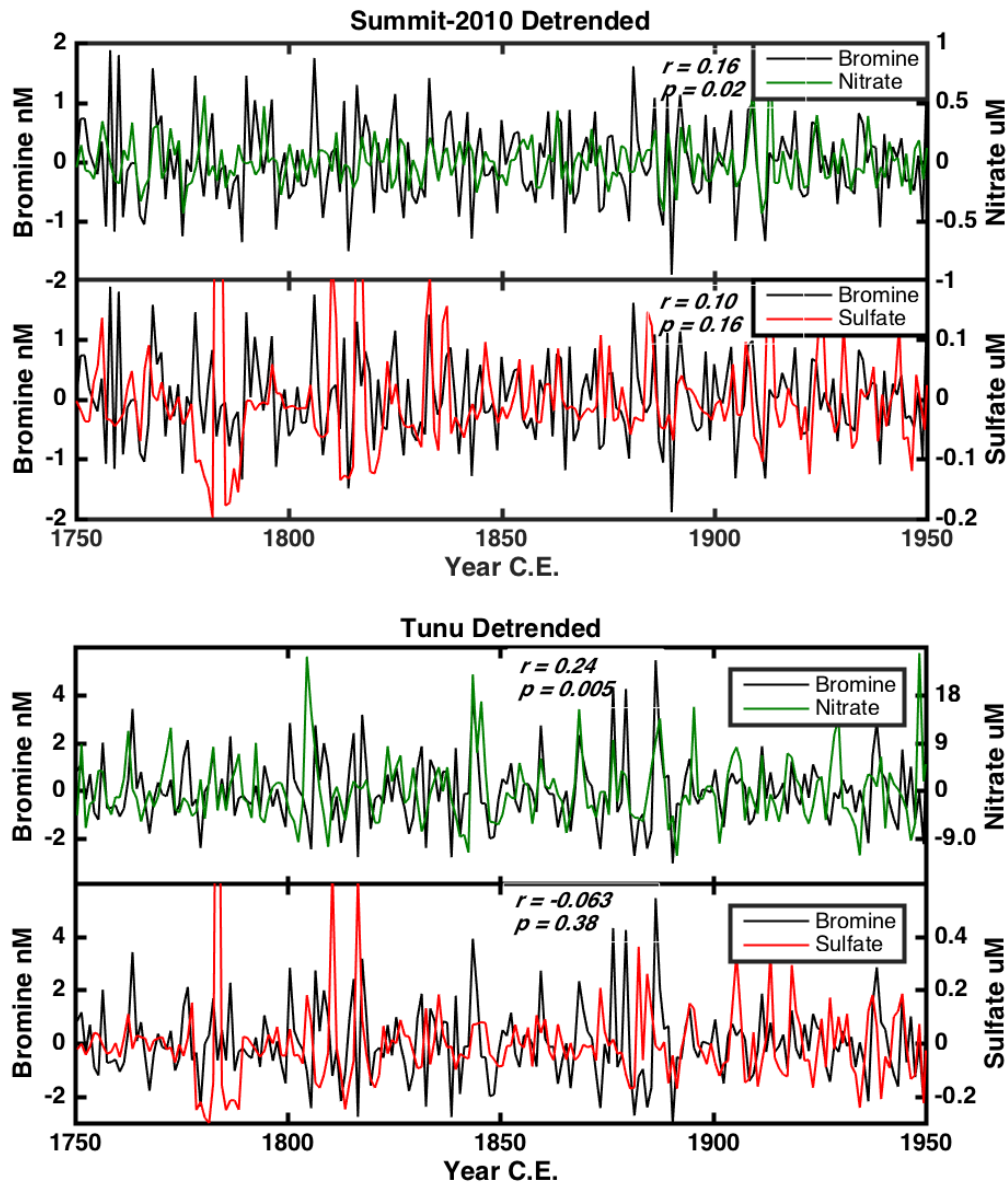
992

993 **Figure 8.** Upper panels: Comparison between bromine in excess of what is expected from a purely sea
 994 ice source (nsiBr, black) and nitrate. The temporal similarities between the nitrate and nsiBr records are
 995 high and indicate that nitrate is a likely driving force for the enhanced release of bromine species from
 996 sea ice sources. Lower panels: Comparison between the calculated nsiBr record and excess lead (exPb,
 997 purple) measured in the ice cores. The lower panels also show the upper limit to the amount of bromine
 998 that could be derived from leaded fuel combustion by assuming exPb:Br ratio of 1:2 after 1925 (blue).
 999 After 1970, when world consumption of leaded gasoline began to fall, nsiBr concentrations continued
 1000 to rise at both ice core sites far above the concentrations that could be explained by leaded gasoline
 1001 sources.

1002

1003

1004



105
106

107 **Figure 9.** High frequency comparison between the annual bromine, nitrate and sulfate records measured
 108 in the ice cores. Each series has been detrended with an 11 year running average before comparison to
 109 remove the low frequency changes in each record. The correlation is highest between bromine and
 110 nitrate at both sites. The r-value for bromine versus nitrate at Summit increases in significance ($r=0.24$,
 111 $p=0.001$) when the entire period (1750-2010) is considered. At both sites there is a close relationship
 112 between the variability in the nitrate and bromine due to their intimate relationship during emission
 113 from the sea ice, transport and deposition onto the snow pack. The correlation between sulfate (or indeed
 114 bulk acidity) and bromine is not significant over any of the time periods shown at either site. Particularly

115 evident is the non-response of the bromine signal to the sulfur rich volcanic events as described in
116 Sect.4.2.2.
117